Study on Surface Complexation of Trace Metal Ions with Metal Oxide Nanoparticles

January 2015

Chiba University
Graduate School of Science
Division of Fundamental Sciences
Department of Chemistry

Naoki Kanaya

(千葉大学審査学位論文)

Study on Surface Complexation of Trace Metal Ions with Metal Oxide Nanoparticles

January 2015

Chiba University
Graduate School of Science
Division of Fundamental Sciences
Department of Chemistry

Naoki Kanaya

Index

List of Figures

List of Tables

1. Introduction

Materials such as metals, semiconductors, and metal oxides, exhibit different physical and chemical properties from bulk materials when the size of the materials is reduced to nanoscale. These properties are considered to be caused from an extremely large specific surface area. These materials are called “nanomaterials” and the technology of nanomaterials is called “nanotechnology”. Nanomaterials have been studied widely as functional materials. The origin of the concept of nanotechnology was Richard P. Feynman’s talk to the American Physical Society in 1959, entitled “There’s Plenty of Room at the Bottom”.[1]

Recent years, metal oxide nanoparticles are widely studied as nanomaterials.[2, 3] For example, alumina nanoparticles are used in a car engine coolant. Titania nanoparticles are used for photocatalysts, cosmetics, and skin care products. Furthermore, metal oxide nanoparticles are used for batteries, antibacterial agents, paints, and so on.[4–7] Magnetic nanoparticles such as iron oxide have been studied to apply for drug delivery systems.[8, 9] In addition, the synthesis of metal oxide nanoparticles has been studied. Nanoparticles can be produced with tunable sizes and shapes by various methods, such as vapor deposition, laser ablation, metal salt reduction, and sol-gel process.[10, 11] Metal oxide nanoparticles also attract attention as low-cost adsorbents for heavy metal ions.[12, 13]

On the other hand, metal oxides such as Al_2O_3 and Fe_2O_3 are naturally present as colloidal nanoparticles in aquatic systems and play an important role in the distribution and diffusion of trace metallic elements in the environment.[14] The mechanism of the adsorption of metal ions on metal oxides is generally explained by complex formation between the surface hydroxyl sites of the oxides and the metal ions in water.[15–18] It has been found that the surface complexation constants of several metal ions to metal oxides and the hydrolysis constants of metal ions show good correlations.[19]

More recently, much attention is focused on metal oxide colloids as factors influencing the behavior of radionuclides in cooling water. Cooling water is used to cool various components such as electromagnets, targets, and particle detectors at particle accelerator facilities. Various radionuclides are produced in the cooling water due to

nuclear reactions under intense radiation field. The generation of radioactive nuclides had not been considered important because the amount was generally extremely small. However, the amount increases with the development of accelerator facilities such as Japan Proton Accelerator Research Complex (J-PARC) at Tokai. Therefore, an appropriate treatment of radionuclides is required. Beryllium-7 (^{7}Be) is one of the most significant gamma-ray emitting nuclides produced in the cooling water. It is important to know the behavior of radioactive and trace ^{7}Be in the cooling water.

High-Energy Accelerator Research Organization (KEK) has been investigating the existing forms and behavior of ^{7}Be. From these investigations, it was found that a part of ^{7}Be was present as fine colloids with diameters of several nanometers.[20-25] These fine colloids had been estimated as metal oxide or metal hydroxide colloids generated by the corrosion of metal components. In the case of the cooling water system for the electromagnets at the 12-GeV proton accelerator facility of KEK, elemental analyses, electron microscope observations, and powder X-ray diffraction spectrometry clarified the dominant colloidal materials to be copper oxide generated through the corrosion of a coil material made of oxygen-free copper.[26] Considering these facts, ^{7}Be is captured by CuO colloidal nanoparticles in the cooling water.

The partition behavior of metal ions on the oxides of divalent metal ions, such as CuO and CoO, consisting of divalent metal ions has not been studied because these metal oxides has been considered less important. The partition behavior of Be(II) on metal oxides has also not been investigated. Because the Be^{2+} ion has the smallest size of all the metal ions, it has a large positive charge density. In order to clarify the tendency and features of the interaction of Be(II) with metal oxides, it is necessary to determine and compare the surface complexation constants for various metal ions and metal oxides. The purpose of this study is to clarify the partition behavior of metal ions to metal oxide nanoparticles as a joint research with High-Energy Accelerator Research Organization (KEK).

In this study, the partition behavior of metal ions (Be(II), Ni(II), and Cu(II)) to nanoparticles of several metal oxides (Al_2O_3, TiO_2, Fe_2O_3, CoO, and CuO) and SiO_2 in water was quantitatively evaluated at 25 ºC. The distribution ratio of the metal ion

between the nanoparticle phase and the aqueous solution phase was measured as a function of aqueous pH, and the complexation equilibria between the metal ion and the surface hydroxyl sites were analyzed. In addition, the zeta potentials and particle size distributions of the nanoparticles dispersed in water were measured. Based on the complexation constants obtained, the factors governing the interaction of metal ions with metal oxides are discussed. The result is expected to understand the role of the metal oxide colloids as the metal ion scavengers.

2. Experimental

2-1 Reagents and chemicals

Nanoparticles of Al_2O_3, SiO_2, TiO_2, Fe_2O_3, CoO, and four kinds of copper oxide were purchased and used as received. Four kinds of copper oxide nanoparticles were denoted as CuO–CIK, CuO–2810NH, CuO–US3063, and CuO–US3065. The manufacturers and some physical properties of these nanoparticles are shown in Table 1. TEM photographs of nanoparticles purchased from C. I. Kasei. Co., Ltd. are shown in Fig. 1. Water was ion-exchanged with a Demi-Ace Model DX-15A (Kurita Water Industries) and furthermore deionized with Milli-Q Labo system (Millipore) just before use. Aqueous standard solutions of Be(II) were purchased from Kanto Chemical as 1005 mg dm^{-3} atomic absorption standards; after they were diluted appropriately and were acidified with nitric acid (final HNO_3 concentration, 0.7 mol dm^{-3}) for atomic absorption spectrometry (AAS). Aqueous standard solutions of Ni(II) were purchased from Kanto Chemical as 1008 mg dm^{-3} atomic absorption standards; after they were diluted appropriately and were acidified with nitric acid (final HNO_3 concentration, 0.1 mol dm^{-3}) for AAS. Aqueous standard solutions of Cu(II) were purchased from Kanto Chemical as 1000 mg dm^{-3} atomic absorption standards; after they were diluted appropriately and were acidified with nitric acid (final HNO_3 concentration, 0.1 mol dm^{-3}) for AAS. As a matrix modifier for graphite furnace AAS (GF-AAS) of Be(II), magnesium nitrate solutions purchased from Wako Chemical as a 10000 mg dm^{-3} atomic absorption standards; were used after appropriate dilution and were acidified with nitric acid (final HNO_3 concentration, 0.4 mol dm^{-3}). Analytical grade potassium hydrogen phthalate was dried at 110 ºC for 4 h before use as a standard for acid-base titrations. Other chemicals were purchased as analytical grade reagents and used without further purification.

2-2 Instruments

The concentration of metal ions in an aqueous phase was determined by GF-AAS with a Hitachi polarized Zeeman atomic absorption photometer Z-5000 and Z-8200.

Table 1. Physical properties of metal oxide nanoparticles cited from supplier's data

	Average particle size (nm)	Density (g cm^{-3})	Specific surface area (m^2 g^{-1})	Purity (%)	Manufacturer
Al_2O_3	31	3.5	50.7	99.9	C. I. Kasei. Co., Ltd
SiO_2	25	2.2	95.4	99.9	C. I. Kasei. Co., Ltd
TiO_2	36	3.7	41.2	99.8	C. I. Kasei. Co., Ltd
Fe_2O_3	39	5.1	26.7	99.5	C. I. Kasei. Co., Ltd
CoO	22	5.4	39.4	99.5	C. I. Kasei. Co., Ltd
CuO−CIK	48	6.3	13.4	99.9	C. I. Kasei. Co., Ltd
CuO−2810NH	40	6.4	～ 20	99	Sky Spring Nanomaterials, Inc.
CuO−US3063	25－55	6.4	13.98	99.95	US Research Nanomaterials, Inc.
CuO−US3065	< 80	6.4	> 18	99.0	US Research Nanomaterials, Inc.

Al_2O_3

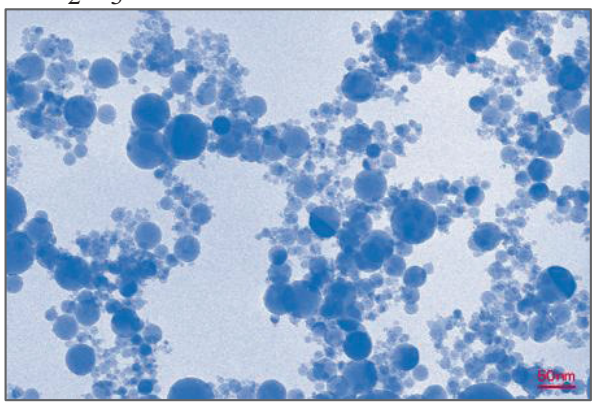

SiO_2

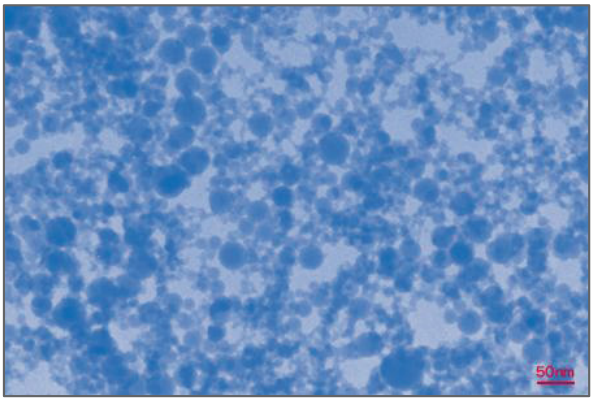

TiO_2

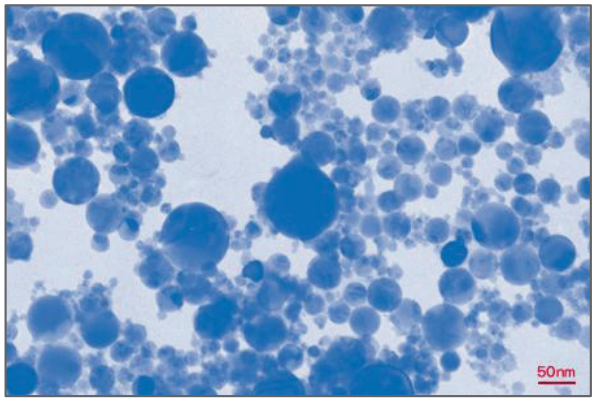

Fe_2O_3

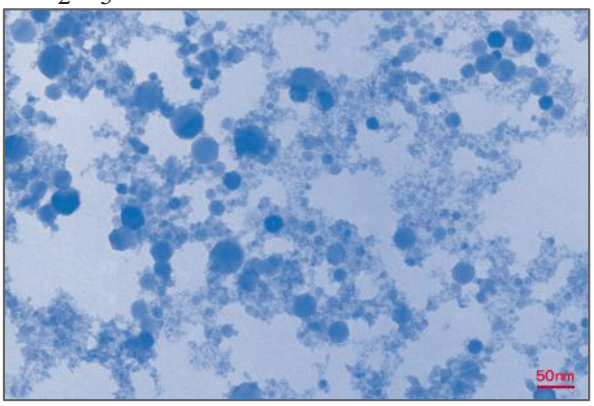

CoO

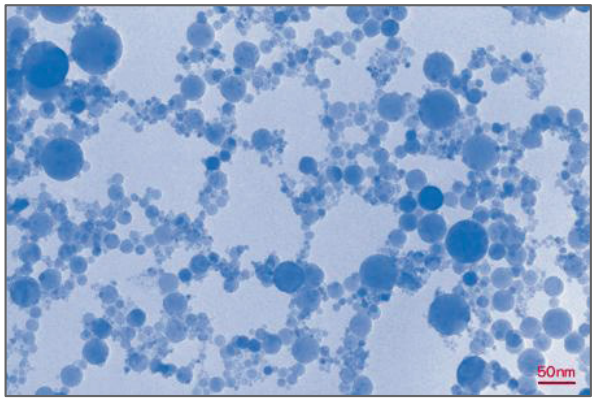

CuO−CIK

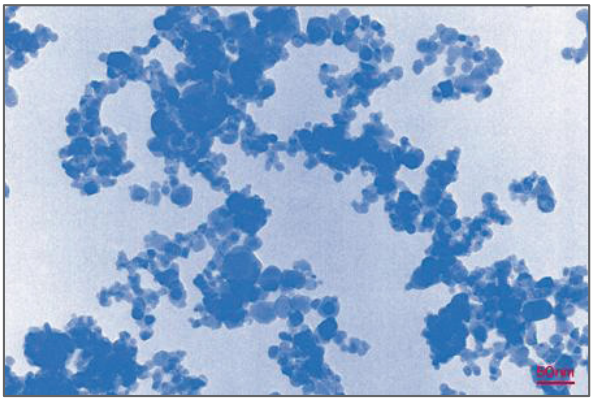

Fig. 1. TEM photographs from CIK NanoTek Corporation of metal oxide nanoparticles, NanoTek®. (http://www.cik.co.jp/product/nanotek/english/nanotek13.html) [cited 2015 Jan]

The zeta potential and particle size distribution of the oxide nanoparticles dispersed in water were measured by laser Doppler electrophoresis and dynamic light scattering using a Horiba SZ-100 nanoparticle analyzer. For the partition experiments of Be(II) with the copper oxide nanoparticles, mechanical shaking and centrifugation were conducted using a Taitec Recipro Shaker SR-1N (190 strokes / min) and a Compact Tabletop Centrifuge Model 2010 (max speed 4000 rpm, relative centrifugal force 2580 × g)[27] with a RS-240 swinging rotor, respectively. Other partition experiments were carried out with a Tokyo Rikakikai Eyela SS-8 (90 strokes / min) and a Micro Refrigerated Centrifuge Model 3700 (max speed 15000 rpm, relative centrifugal force 22140 × g)[28] with an AF-5004CH angle rotor.

2-3 Partition experiments of metal ions between nanoparticles and aqueous phase

Aqueous solutions that containing a metal ion (Be(II), Ni(II), or Cu(II)) were prepared as follows. Concentrations of Be(II), Ni(II), and Cu(II) were 1.00×10^{-7} mol dm^{-3}, 8.57×10^{-6} mol dm^{-3}, and 7.87×10^{-6} mol dm^{-3}, respectively. The pH of each solution was adjusted with CH_3COOH–CH_3COONa buffer (pH 3.7 to 5.3) or 2-morpholinoethanesulfonic acid (MES)–NaOH buffer (pH 5.3 to 6.5). Ionic strength was adjusted to 0.01 using $NaNO_3$. Concentrations of the buffer components were as follows: CH_3COOH 5.0×10^{-4}–5.0×10^{-3} mol dm^{-3}; CH_3COONa 1.0×10^{-3}–5.0×10^{-3} mol dm^{-3}; MES 1.0×10^{-2} mol dm^{-3}; NaOH 2.0×10^{-3}–8.0×10^{-3} mol dm^{-3}. The buffer solution of the metal ion (20 cm^3) was mixed with the oxide nanoparticles (0.001–1 g) in a plastic vial. The vial was mechanically shaken for 3–72 h at 25 ± 0.2 ºC. For the partition experiments of Be(II) with CuO–CIK, the CuO–CIK nanoparticles were removed from the suspension by using a centrifugation-type ultrafiltration unit (Vivascience Vivaspin 20; MWCO 1000 kDa) with an estimated pore size of 16 nm based on the correlation between the molecular weight and estimated molecular size.[29] For the partition experiments of Be(II) with CuO–2810NH, CuO–US3063, and CuO–US3065, the copper oxide nanoparticles were removed from the suspension by centrifugation at 3500 rpm. For other experiments, the nanoparticles were removed

from the suspension by centrifugation at 15000 rpm. The concentration of the metal ion in the aqueous phase was determined by GF-AAS, and the distribution ratio of the metal ion between the nanoparticle phase and the aqueous solution phase was calculated. In order to evaluate an effect of ionic strength on the partition of Be(II) to CuO–CIK, the partition experiments were performed for both the solutions of ionic strength 0.002–0.007 and 0.1.

2-4 Measurement of surface hydroxyl site concentration on oxide nanoparticles

The surface hydroxyl concentration per unit mass of the oxide nanoparticles was determined as follows. A nanoparticles (0.5 g) / water (50 cm^3) suspension was placed in a glass beaker and stirred with a magnetic stirrer in a temperature-controlled water bath (25 ± 0.2 ºC). Acid-base titration experiments were performed by successive addition of aliquots of a calibrated aqueous NaOH solution (1.11×10^{-2}–1.23×10^{-2} mol dm^{-3}), an aqueous HCl solution (4.11×10^{-3} mol dm^{-3}) or an aqueous H_2SO_4 solution (7.87×10^{-3} mol dm^{-3}) to the suspension. The HCl solution was used for Fe_2O_3 and the H_2SO_4 solution was used for CuO–2810NH, CuO–US3063, and CuO–US3065, respectively. The pH of the suspension was measured with a glass electrode. Blank experiment was carried out using the same amount of pure water instead of the nanoparticles / water suspension. By comparing the titration curves of the nanoparticles / water suspension and pure water, the surface hydroxyl concentration per unit mass of nanoparticles (mol g^{-1}) was determined. The NaOH solution was standardized using potassium hydrogen phthalate. The HCl and H_2SO_4 solutions were calibrated using the standard NaOH solution.

2-5 Measurements of zeta potential and particle size distribution

2-5-1 Preparation of sample solution

The nanoparticles / water suspension was prepared and the pH of each solution was adjusted with 3×10^{-4} mol dm^{-3} HCl solution (pH 3.6), 1.5×10^{-2} mol dm^{-3} potassium hydrogen phthalate–HCl buffer (pH 4.1), 5×10^{-3} mol dm^{-3} CH_3COOH–CH_3COONa

buffer (pH 4.7), 1×10^{-2} mol dm^{-3} MES–NaOH buffer (pH 5.5 to 6.7), 2×10^{-3} mol dm^{-3} 1,4-piperazinediethanesulfonic acid (PIPES)–NaOH buffer (pH 7.2), 1×10^{-3}–2×10^{-2} mol dm^{-3} NH_3–NH_4Cl buffer (pH 7.9 to 10.2), or 1×10^{-3} mol dm^{-3} NaOH solution (pH 10.9). Ionic strength was adjusted to 0.01 using $NaNO_3$.

2-5-2 Measurement of zeta potential of nanoparticles dispersed in water

The zeta potential of the oxide nanoparticles dispersed in water were measured by laser Doppler electrophoresis. A charged nanoparticle is moved by an applied electric field. This motion speed is proportional to the charge of the nanoparticle and can be measured by light scattering. The nanoparticle is illuminated with laser light and therefore the nanoparticle scatters the light. The frequency of the scattered light is a function of the nanoparticle velocity due to the Doppler shift. From the applied electric field and measured nanoparticle velocity, the nanoparticle mobility is determined. The zeta potential is then calculated from the mobility.[30] A measurement cell used was a carbon electrode cell and the voltage applied to the electrodes was set to 3.4 V. For each nanoparticle, the nanoparticles / water suspensions were prepared as follows: Al_2O_3 100 mg dm^{-3}; SiO_2, TiO_2, Fe_2O_3, CuO–CIK, CuO–US3063 and CuO–US3065 200 mg dm^{-3}; CoO 180 mg dm^{-3}; CuO–2810NH 500 mg dm^{-3}. The zeta potential was measured as a function of pH.

2-5-3 Measurement of particle size distribution of nanoparticles dispersed in water

The particle size distribution of the oxide nanoparticles dispersed in water were measured by dynamic light scattering. Nanoparticles dispersed in water undergo thermal motion known as Brownian motion. The nanoparticle is illuminated with laser light and therefore the nanoparticle scatters the light. The scattered light is collected with a detector. By analyzing the signal, the diffusion coefficient of the nanoparticles is determined and the Stokes-Einstein equation is then used to calculate the nanoparticle size.[30] For each nanoparticle, the nanoparticles / water suspensions were prepared as

follows: Al_2O_3 100 mg dm^{-3}; SiO_2 150 mg dm^{-3}; TiO_2 25 mg dm^{-3}; Fe_2O_3 and CoO 60 mg dm^{-3}; CuO–CIK, CuO–2810NH, CuO–US3063, and CuO–US3065 1000 mg dm^{-3}. The particle size was measured as a function of pH. A measurement cell used was a 1 cm square cell. The scattered light was collected by a detector with either 90º or 173º scattering angle.

3. Results and Discussion

In this section, the partition behavior of a metal ion to the nanoparticles of several metal oxides and SiO_2 in water is quantitatively explained on the basis of the complexation model between the metal ion and surface hydroxyl sites of the oxides. The partition behavior of the metal ion was evaluated as a function of pH. In addition, the zeta potentials, average particle sizes, and surface hydroxyl site concentrations were determined for the nanoparticles in an aqueous suspension state. Based on the experimental results, the surface complexation constants were determined. The tendency of the surface complexation constants is discussed based on the properties of the oxide nanoparticles or the metal ion in water.

3-1 Partition behavior of metal ion in nanoparticle dispersed aqueous solution

3-1-1 Partition behavior of Be(II) in nanoparticle dispersed aqueous solution

The partitioning of the metal ion between the nanoparticle phase and the aqueous solution phase was evaluated in terms of the distribution ratio (D) defined by Eq. (1):

$$D = \frac{\text{Concentration of the metal ion in the nanoparticle phase (mol g}^{-1}\text{)}}{\text{Concentration of the metal ion in the aqueous solution phase (mol dm}^{-3}\text{)}}. \quad (1)$$

First, preliminary investigations were carried out in order to find the suitable amount of the nanoparticles for the partition experiments when the volume of the aqueous solution phase was fixed to 20 cm^3. When the buffer solution of 1.00×10^{-7} mol dm^{-3} Be(II) was mixed with oxide nanoparticles (0.5 g) in a plastic vial, except for CuO–CIK and CuO–2810NH, most of Be(II) was distributed to the nanoparticles and the concentration of Be(II) in aqueous phase was less than the detection limit of GF-AAS. Thus, the amount (0.5 g) of the nanoparticles used for the partition experiments was too large. In the case of CuO–CIK and CuO–2810NH, the amount (0.5

g) of the nanoparticles was suitable for the evaluation of the distribution ratio. Finally, the suitable amount of the nanoparticles was found to be 0.001–0.02 g for Al_2O_3, SiO_2, TiO_2, and Fe_2O_3; 0.02–0.2 g for CoO; 0.5 g for CuO–CIK and CuO–2810NH; 0.05 g for CuO–US3063, and CuO–US3065.

Second, the distribution ratio of Be(II) to the nanoparticles was measured as a function of the shaking time at a fixed pH (pH 5.8). The results are shown in Fig. 2. Although in the case of using SiO_2 nanoparticles the distribution ratio gradually decreases with the shaking time from 3 to 48 h, a constant distribution ratio is obtained over 48 h. In the case of using other nanoparticles, the shaking time required to obtain a constant distribution ratio is about 24 h. In the following study, the shaking time was fixed to 48 h for all the nanoparticles.

Third, the pH dependence of the distribution ratio was investigated. The pH of the aqueous solution phase was varied by using CH_3COOH–CH_3COONa or MES–NaOH buffers. In Fig. 3, logarithmic values of *D* are shown as a function of pH. For all the oxide nanoparticles, the log *D* value increases with increasing pH. The *D* value at pH 6.0 varies in the order $Fe_2O_3 \approx TiO_2 \approx SiO_2 > Al_2O_3 >> CoO >$ CuO–US3063 > CuO–US3065 > CuO–CIK > CuO–2810NH. Although the *D* value takes the different value by the nanoparticles, four types of CuO nanoparticles show relatively similar values. This result suggests that the distribution behavior of Be(II) on the nanoparticles are not largely affected by the difference of CuO nanoparticle species. As an overall trend, the *D* value is larger for the oxide in which the metal (including Si) has a higher valence. This order is not consistent with that of the surface hydroxyl site concentration (mol g^{-1}) of the metal oxide, i.e., $CoO > SiO_2 \approx$ CuO–US3063 $\approx Al_2O_3 >$ CuO–US3065 $> TiO_2 > Fe_2O_3 >$ CuO–CIK > CuO–2810NH (Table 2).

There was no correlation between the order of *D* value and that of the physical properties of the nanoparticles such as average particle diameters and specific surface area under a dry state shown in Table 1. These results have suggested that some other factors play an important role in the partition behavior of Be(II) to the oxide nanoparticles dispersed in water. The factors governing the partition behavior are discussed in detail in section 3-5.

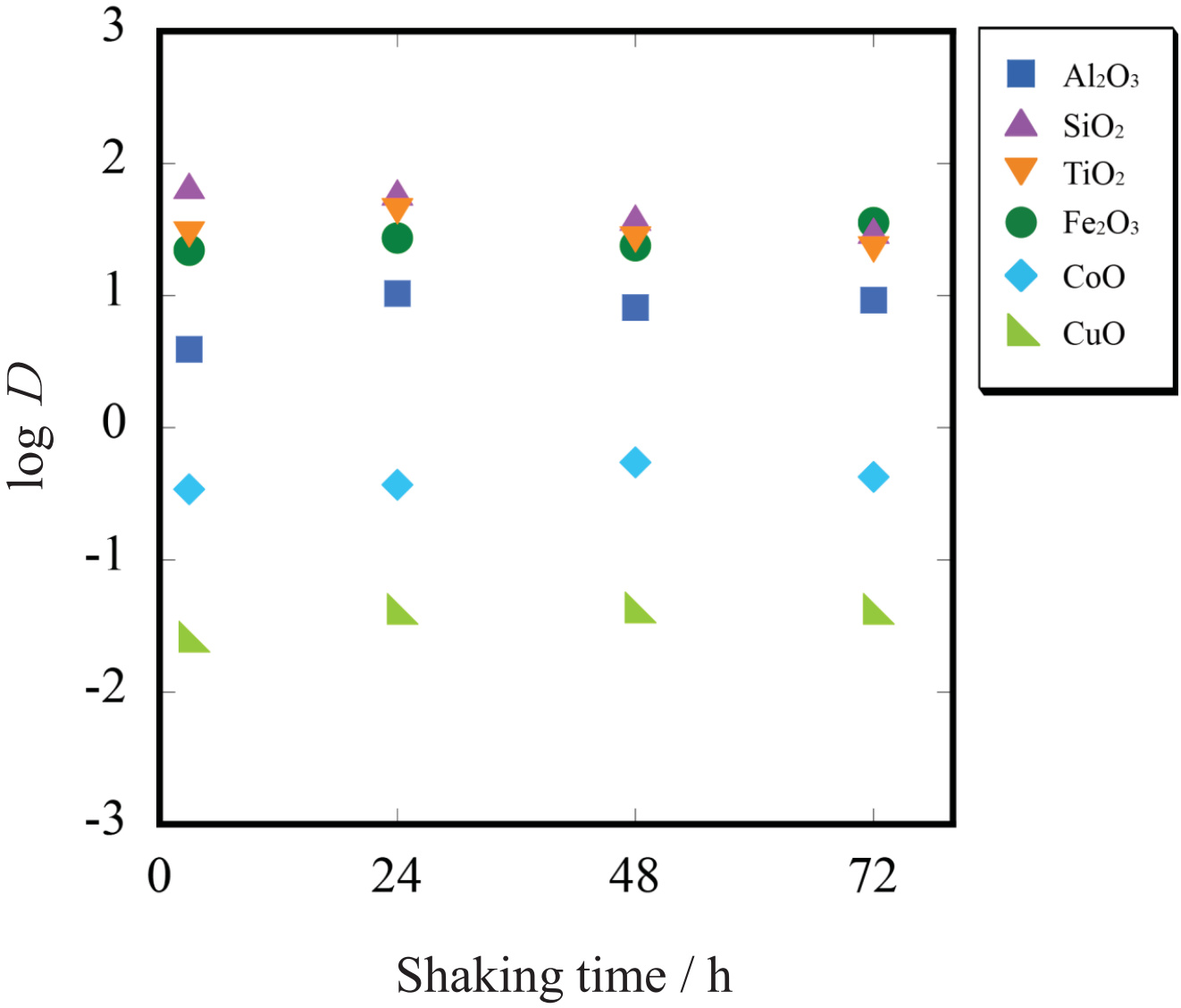

Fig. 2. Plots of log D for the distribution of Be(II) on metal oxide nanoparticles in water as a function of shaking time. Al_2O_3, Fe_2O_3, SiO_2, TiO_2: 0.001–0.002 g, CoO: 0.02 g, CuO(CuO−CIK): 0.50 g; Aq. soln.: 20 cm^3; Initial Be(II) concentration: 7.0×10^{-8}–8.5×10^{-8} mol dm^{-3}; pH 5.8; Shaking time: 3–72 h.

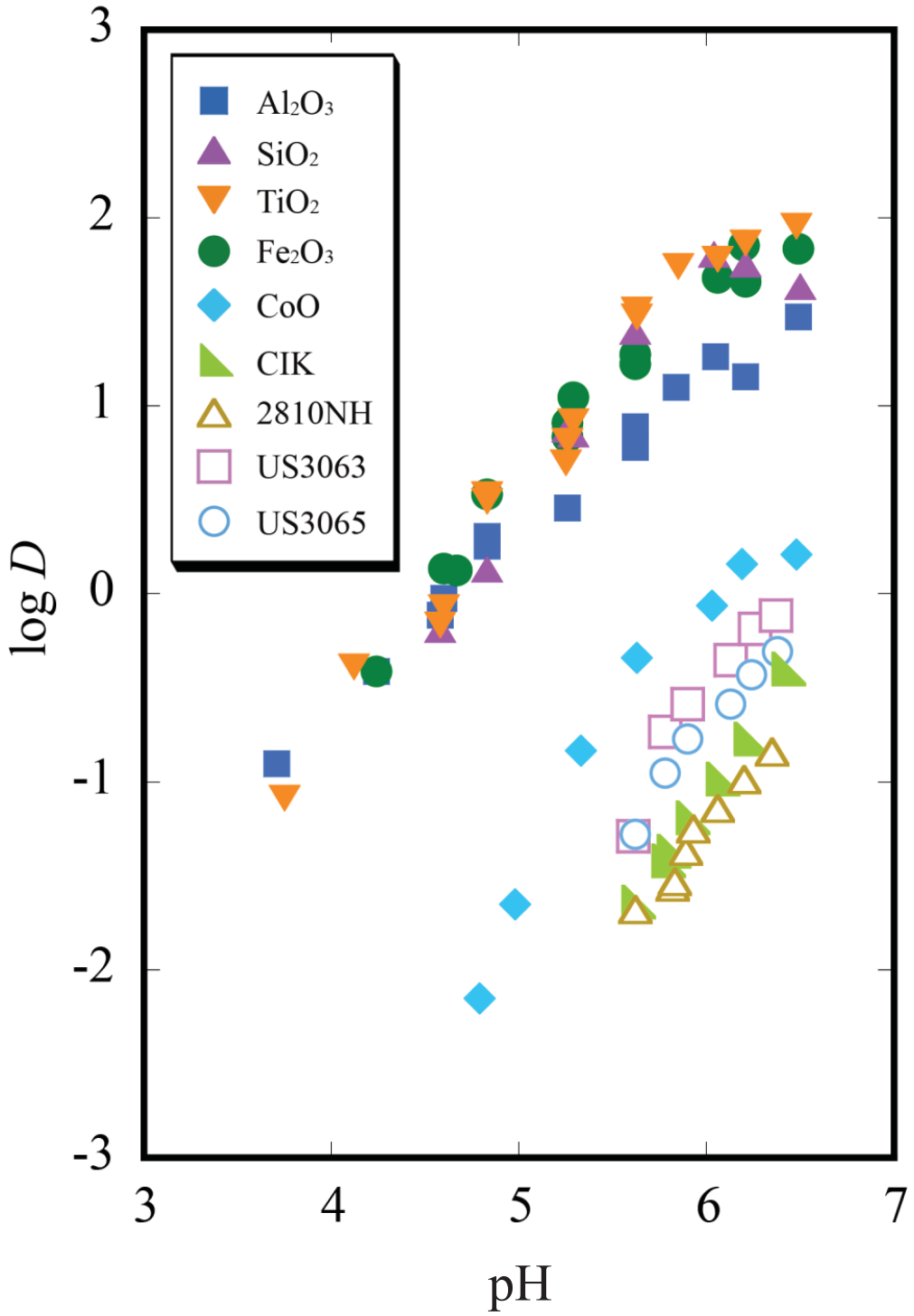

Fig. 3. Plots of log *D* for the distribution of Be(II) on metal oxide nanoparticles in water as a function of pH.
Al_2O_3, SiO_2, TiO_2, Fe_2O_3: 0.001–0.02 g, CoO: 0.02–0.2 g, CuO−CIK, CuO−2810NH: 0.5 g, CuO−US3063, CuO−US3065: 0.05 g; Aq. soln.: 20 cm^3; Initial Be(II) concentration: 4.6×10^{-8} –1.0×10^{-7} mol dm^{-3}; pH 3.7–6.5; Shaking time : 48 h.

Moreover, the ionic strength dependence of the distribution ratio was investigated. The buffer solution of 1.00×10^{-7} mol dm^{-3} Be(II) was prepared and ionic strength was 0.002–0.007 without $NaNO_3$ and 0.1 with $NaNO_3$. In the calculation of the ionic strength, the contribution of Be(II) was negligible. The buffer solution (20 cm^3) was mixed with CuO–CIK (0.5 g) in a plastic vial and mechanically shaken for 48 h. The results are shown in Fig. 4. The difference between the results at a lower ionic strength and those at a higher ionic strength is small. Hence, the partition behavior of Be(II) is found to be hardly dependent on the ionic strength of the aqueous solution.

3-1-2 Partition behavior of Ni(II) in nanoparticle dispersed aqueous solution

First, preliminary investigations were carried out in order to find the suitable amount of the nanoparticles for the partition experiments when the volume of the aqueous solution phase was fixed to 20 cm^3. The buffer solution of 8.57×10^{-6} mol dm^{-3} Ni(II) was mixed with six types of various oxide nanoparticles (0.5 g) in a plastic vial and the distribution ratio was determined. From the evaluation of the distribution ratio, the suitable amount of the nanoparticles was found to be 0.5–1 g for Al_2O_3; 0.05–0.5 g for TiO_2; 0.5 g for Fe_2O_3 and CoO. In the case of SiO_2 and CuO–CIK nanoparticles, the distribution of Ni(II) could not be detected.

Second, the pH dependence of the distribution ratio was investigated. The pH of the aqueous solution phase was varied by using MES–NaOH buffers. In Fig. 5, the log *D* are shown as a function of pH. For all the oxide nanoparticles, the log *D* value increases with increasing pH. The *D* value at pH 6.0 varies in the order $TiO_2 > Fe_2O_3 > CoO > Al_2O_3$. This order is not consistent with that of the *D* value of Be(II) with the metal oxide nanoparticles.

There was no correlation between the order of *D* value and that of the physical properties of the nanoparticles such as average particle diameters and specific surface area under a dry state shown in Table 1. These results have suggested that some other factors play an important role in the partition behavior of Ni(II) to the oxide nanoparticles dispersed in water. The factors governing the partition behavior are

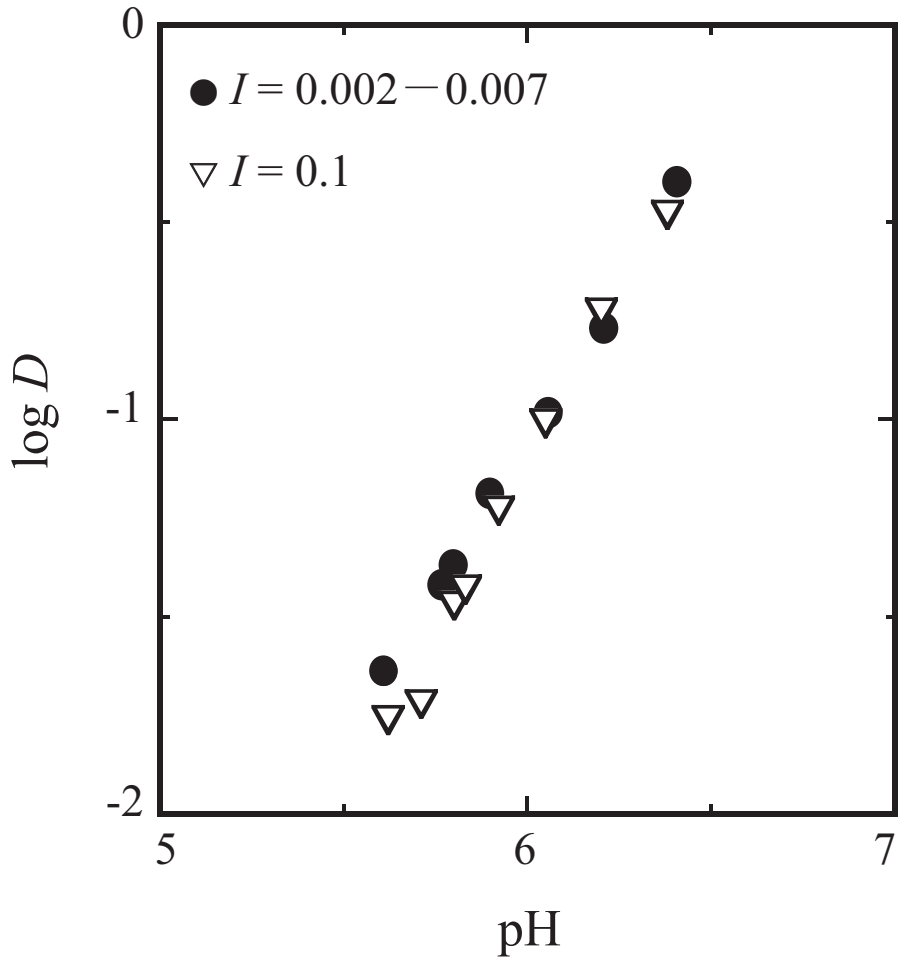

Fig. 4. Effect of ionic strength on log *D* for the distribution of Be(II) on CuO nanoparticles (CuO−CIK) in aqueous solution as a function of pH.
CuO nanoparticles (CuO−CIK): 0.50 g; Aq.soln.: 20 cm^3;
Initial Be(II) concentration : 5.6×10^{-8}–9.6×10^{-8} mol dm^{-3};
pH 5.6–6.4 ; Shaking time : 48 h.

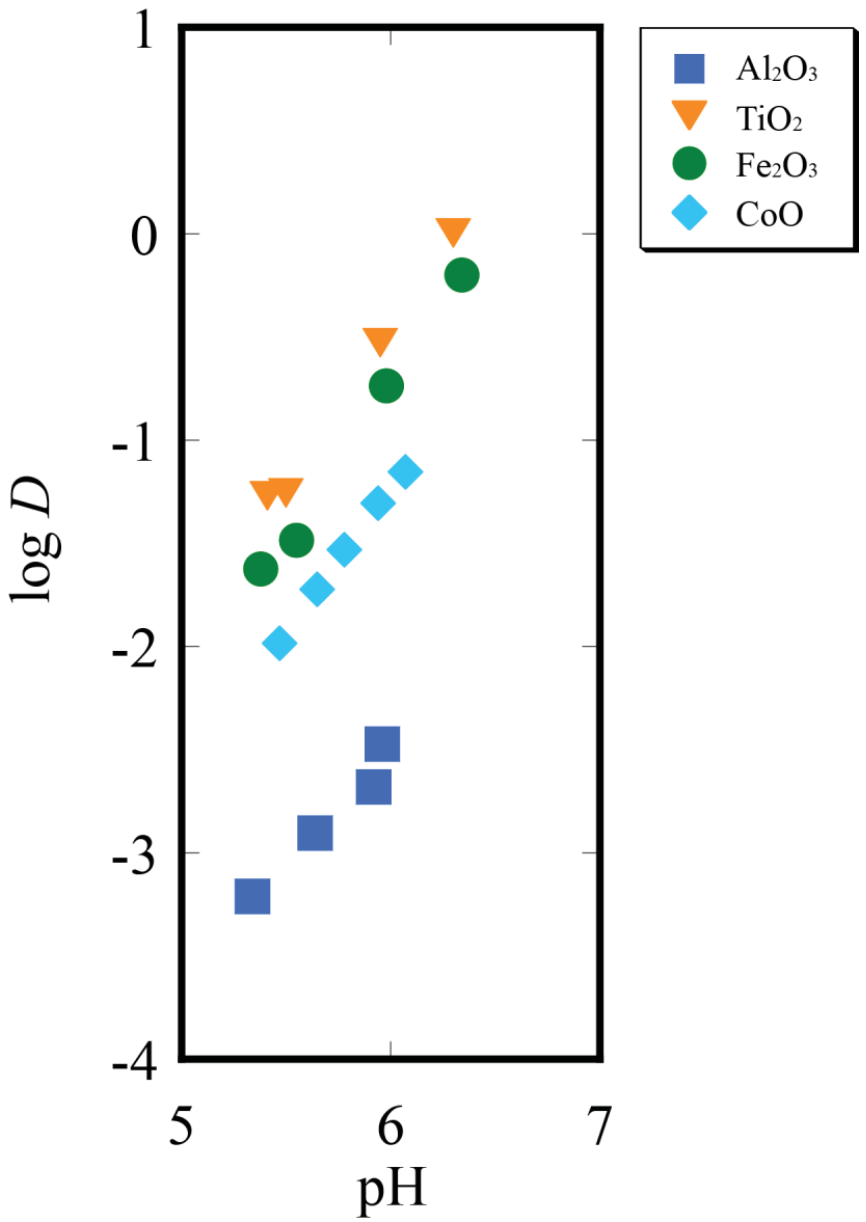

Fig. 5. Plots of log D for the distribution of Ni(II) on metal oxide nanoparticles in water as a function of pH.
Al_2O_3: 0.5–1 g, TiO_2: 0.05–0.5 g, Fe_2O_3, CoO: 0.5 g; Aq. soln.: 20 cm^3; Initial Ni(II) concentration: 1.9×10^{-7}–8.9×10^{-6} mol dm^{-3}; pH 5.3–6.3; Shaking time: 48 h.

discussed in detail in section 3-5.

3-1-3 Partition behavior of Cu(II) in nanoparticle dispersed aqueous solution

First, preliminary investigations were carried out in order to find the suitable amount of the nanoparticles for the partition experiments when the volume of the aqueous solution phase was fixed to 20 cm^3. The buffer solution of 7.87×10^{-6} mol dm^{-3} Cu(II) was mixed with oxide nanoparticles (0.5 g) in a plastic vial and, except for SiO_2, most of Cu(II) was distributed to the nanoparticles and the concentration of Cu(II) in aqueous phase was less than the detection limit of GF-AAS. Thus, the amount (0.5 g) of the nanoparticles used for the partition experiments was too large. In the case of SiO_2, the amount of Cu(II) distributed to the nanoparticle was too small for the evaluation of the distribution ratio. In addition, the trace amount of CuO–CIK nanoparticle was found to be dissolved in the aqueous phase. Although the amount was very small, the effect of the dissolved CuO–CIK nanoparticle on the partition experiments was not negligible. Finally, the suitable amount of the nanoparticles was found to be 0.02 g for Al_2O_3; 1 g for SiO_2; 0.01 g for TiO_2; 0.01–0.02 g for Fe_2O_3 and CoO; the partition experiments for CuO–CIK was abandoned.

Second, the pH dependence of the distribution ratio was investigated. The pH of the aqueous solution phase was varied by using MES–NaOH buffers. In Fig. 6, for all the oxide nanoparticles, the log *D* are shown as a function of pH and increases with increasing pH like the case of Be(II) and Ni(II). The *D* value at pH 6.0 varies in the order CoO > TiO_2 > Fe_2O_3 > Al_2O_3 > SiO_2. Unlike the case of Be(II) and Ni(II), CoO shows the largest *D* value. This order is not consistent with that of the *D* value of Be(II) with the metal oxide nanoparticles. The order of TiO_2, Fe_2O_3, and Al_2O_3 is similar to that of the *D* value of Ni(II).

The correlation between the order of *D* value and that of the properties of the nanoparticles such as average particle diameters and specific surface area under a dry state shown in Table 1 is not clarified. These results have suggested that some other factors play an important role in the partition behavior of Cu(II) to the oxide

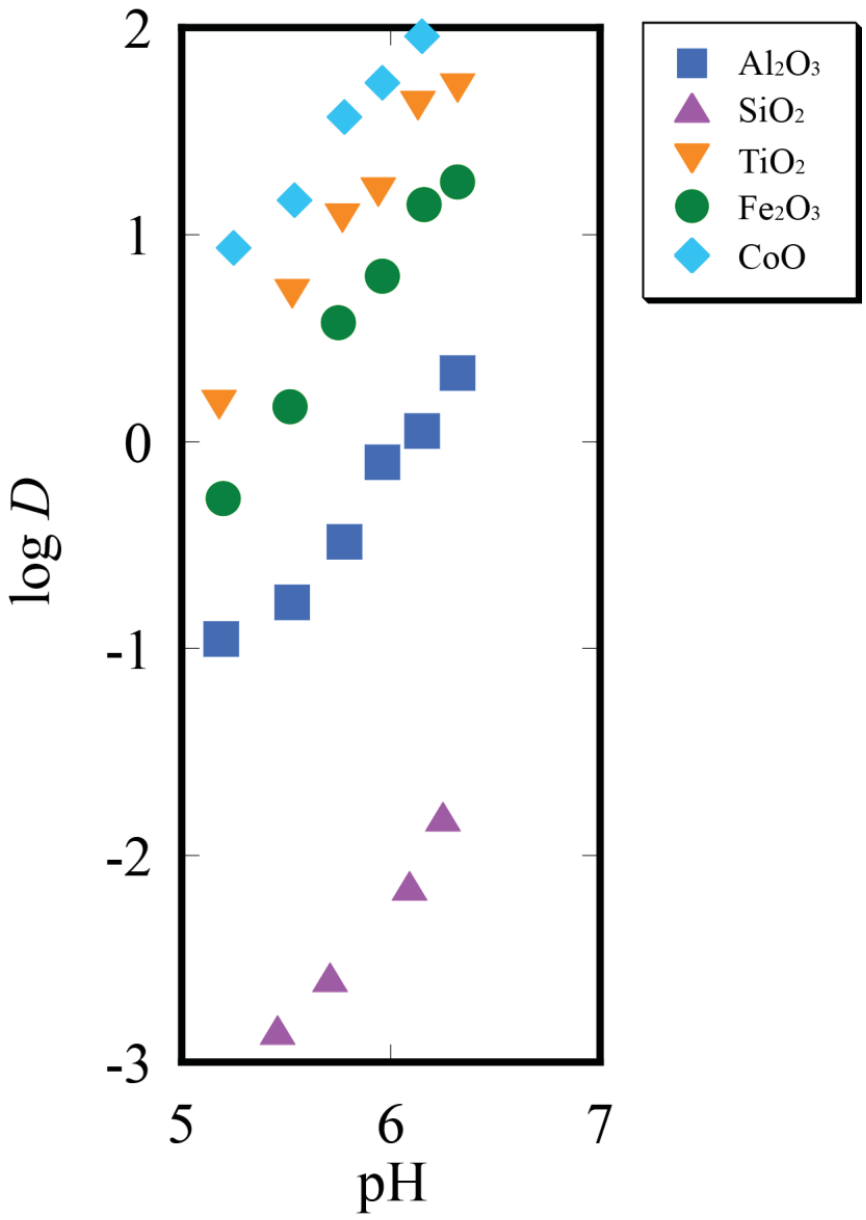

Fig. 6. Plots of log *D* for the distribution of Cu(II) on metal oxide nanoparticles in water as a function of pH.
Al_2O_3: 0.02 g, SiO_2: 1 g, TiO_2: 0.01 g, Fe_2O_3, CoO: 0.01–0.02 g; Aq. soln.: 20 cm^3; Initial Cu(II) concentration: 6.7×10^{-6}–8.6×10^{-6} mol dm^{-3} ; pH 5.2–6.3; Shaking time: 48 h.

nanoparticles dispersed in water. The factors governing the partition behavior are discussed in detail in section 3-5.

3-2 Determination of surface hydroxyl site concentration

3-2-1 Theory

It is known that the acid-base properties of the hydroxyl sites on the oxide surfaces in water can be expressed by the following equations: [15-19, 31]

$$>S\text{-}OH + H^+ \quad \rightleftarrows \quad >S\text{-}OH_2^+, \tag{2}$$

$$>S\text{-}OH + OH^- \quad \rightleftarrows \quad >S\text{-}O^- + H_2O, \tag{3}$$

where >S denotes the solid surface. The hydroxyl site concentration ($[>S\text{-}OH]_S$) is represented as follows:

$$[>S\text{-}OH]_{S\,,\,Total} = [>S\text{-}OH_2^+]_S + [>S\text{-}OH]_S + [>S\text{-}O^-]_S. \tag{4}$$

In the high pH region, it can be considered that most of the hydroxyl sites are deprotonated and were present in the form of $>S\text{-}O^-$. The hydroxyl site concentration can be expressed by the following equations:

$$[>S\text{-}OH]_{S,\,Total} \fallingdotseq [>S\text{-}O^-]_S. \tag{5}$$

By comparing the titration curves of the nanoparticles / water suspension and pure water, the surface hydroxyl site concentration per unit mass of nanoparticles (mol g^{-1}) was determined as follows:

$$[>S\text{-}OH]_S = \Delta x \text{ (mol)} / \text{the amount of the nanoparticles (g)}, \tag{6}$$

where Δx denotes the difference of the amount of sodium hydroxide added between the suspension and pure water at the same pH.

3-2-2 Determination of surface hydroxyl site concentration

The nanoparticles / water suspension was prepared and the pH was measured. The pH values were 4.60, 4.72, 3.44, 6.40, 4.54, 5.98, 6.40, 6.43, 6.70, and 5.75 for Al_2O_3, SiO_2, TiO_2, Fe_2O_3, CoO, CuO–CIK, CuO–2810NH, CuO–US3063, CuO–US3065, and pure water, respectively. In Fig. 7, the titration curves of four kinds of CuO nanoparticles are shown. In Fig. 8, the results of other nanoparticles are shown. By comparing the titration curves of the nanoparticles / water suspension and pure water, the surface hydroxyl site concentration per unit mass of nanoparticles (mol g^{-1}) was determined by Eq. (6) and are summarized in Table 2.

The surface hydroxyl site concentration varies in the order CoO > SiO_2 ≈ CuO–US3063 ≈ Al_2O_3 > CuO–US3065 > TiO_2 > Fe_2O_3 > CuO–CIK > CuO–2810NH. The largest $[>S\text{-}OH]_S$ value is three times larger than the smallest value. The $[>S\text{-}OH]_S$ values are relatively similar to each other, considering the difference of the distribution ratio of the metal ions. Among the four copper oxides, the *D* value of Be(II) is larger for the copper oxide having a higher surface hydroxyl site concentration. However, among all of the nanoparticles, the order of the *D* is not consistent with that of the surface hydroxyl site concentration of the metal oxide.

3-3 Zeta potential

In Fig. 9, the zeta potentials of the four kinds of CuO nanoparticles are shown as a function of pH at a constant ionic strength of 0.01. The results of other nanoparticles are shown in Fig. 10. In all cases, the zeta potential shows a continuous decrease with pH. This result indicates that the degree of dissociation of the hydroxyl sites on the nanoparticle surface changes with the pH as shown by Eqs. (2) and (3). Under the same pH condition as that of the partition experiments (pH 3.7–6.5), the zeta potential value differs depending on the kind of oxide: Al_2O_3 (positive) > CoO, CuO–CIK, CuO–2810NH, CuO–US3063, and CuO–US3065 (positive ~ neutral) > TiO_2 (positive ~ neutral ~ negative) > SiO_2 and Fe_2O_3 (negative).

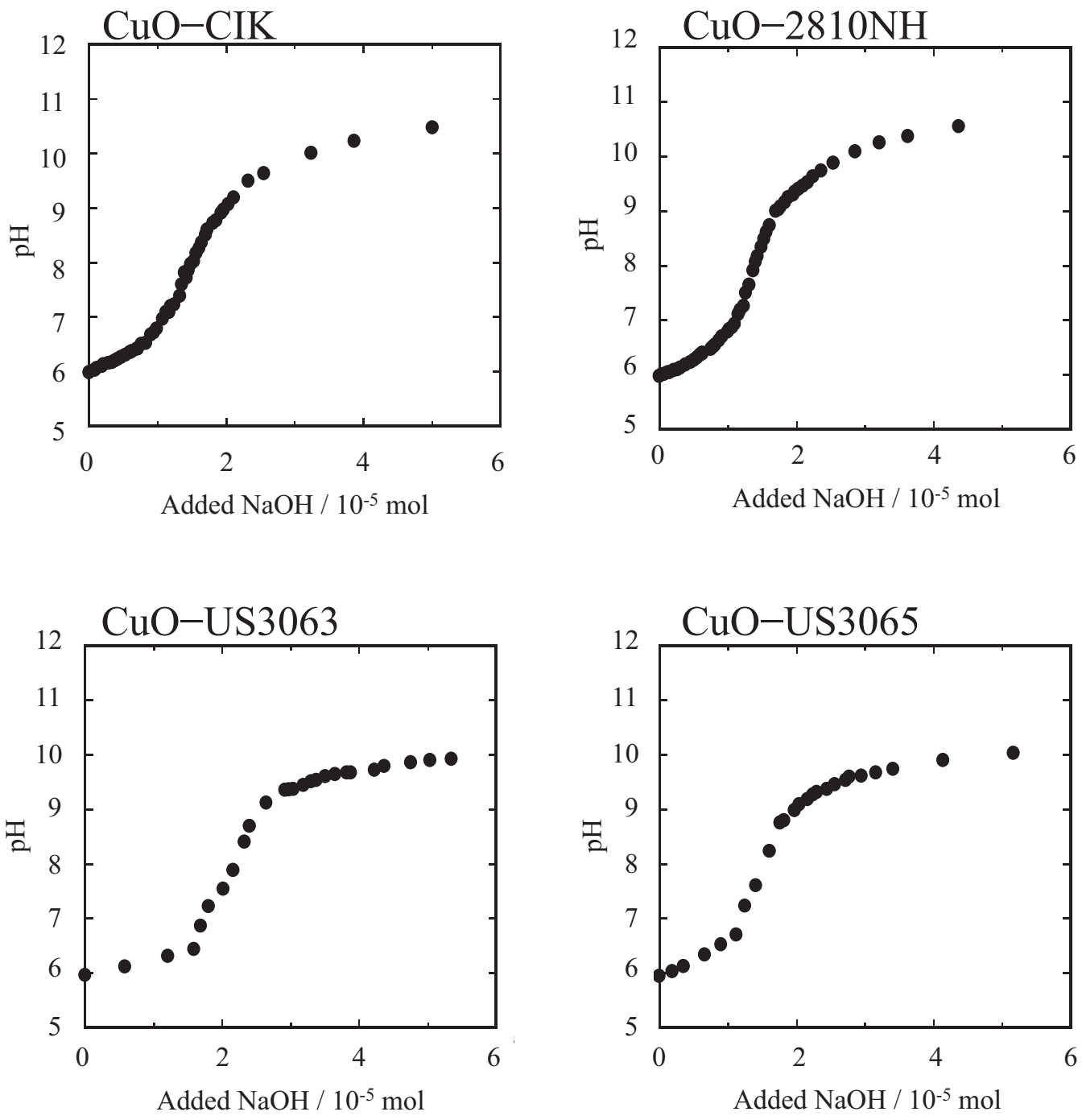

Fig. 7. The pH titration curves of copper oxide nanoparticles in water measured by adding aqueous NaOH solution.
Nanoparticles: 0.01 g cm^{-3};
Added solution: 1.23×10^{-2} mol dm^{-3} NaOH.

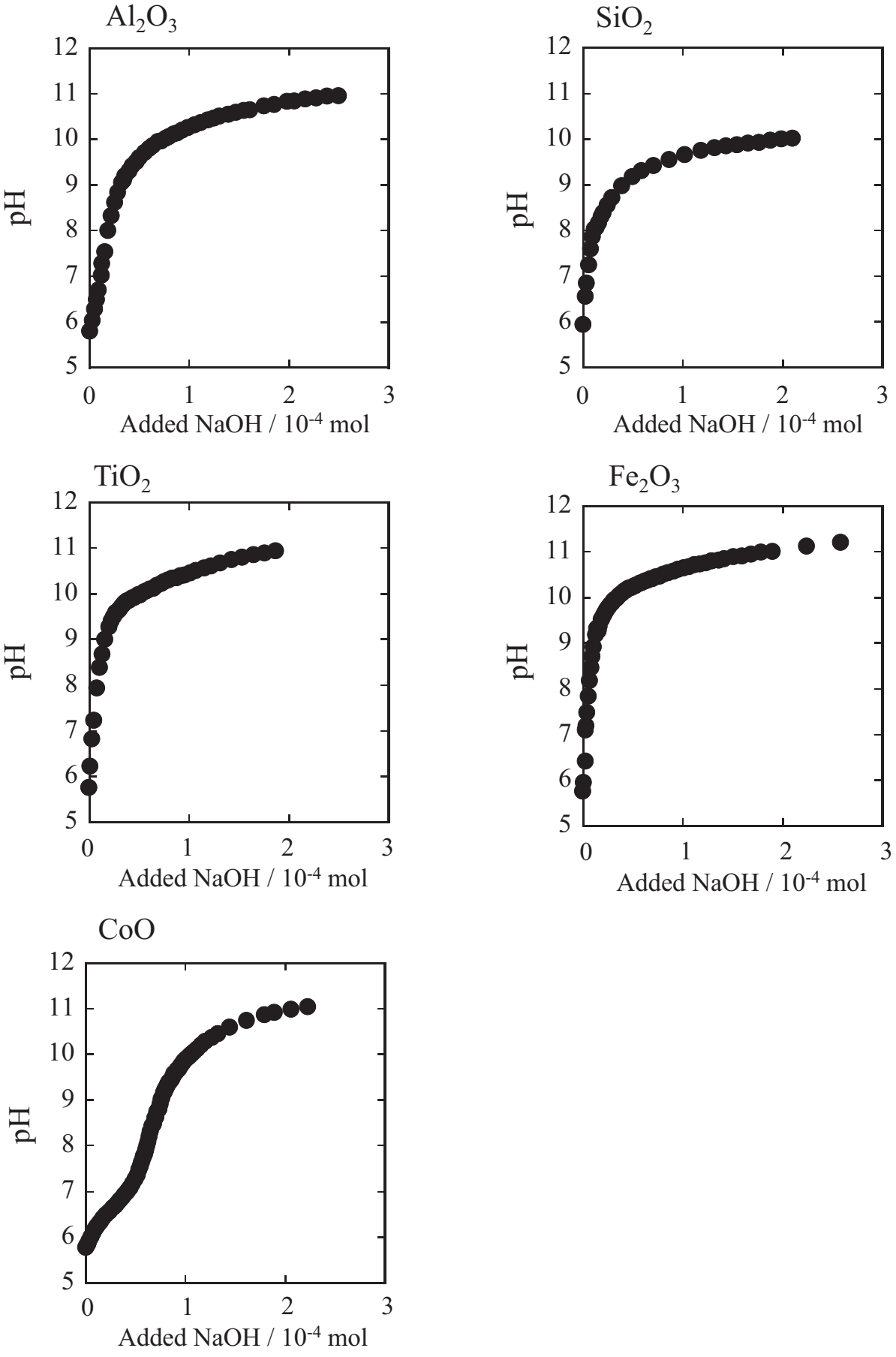

Fig. 8. The pH titration curves of metal oxide nanoparticles in water measured by adding aqueous NaOH solution.
Nanoparticles: 0.01 g cm^{-3};
Added solution: 1.11×10^{-2} mol dm^{-3} NaOH.

Table 2. Surface hydroxyl site concentrations ($[>S\text{-}OH]_S$) for metal oxide nanoparticles

	$[>S\text{-}OH]_S$ (mol g^{-1})
Al_2O_3	$(1.09 \pm 0.08) \times 10^{-4}$
SiO_2	$(1.2 \pm 0.2) \times 10^{-4}$
TiO_2	$(7.2 \pm 0.4) \times 10^{-5}$
Fe_2O_3	$(4.9 \pm 0.4) \times 10^{-5}$
CoO	$(1.83 \pm 0.02) \times 10^{-4}$
CuO−CIK	$(3.7 \pm 0.1) \times 10^{-5}$
CuO−2810NH	$(3.3 \pm 0.1) \times 10^{-5}$
CuO−US3063	$(1.1 \pm 0.1) \times 10^{-4}$
CuO−US3065	$(8.0 \pm 0.2) \times 10^{-5}$

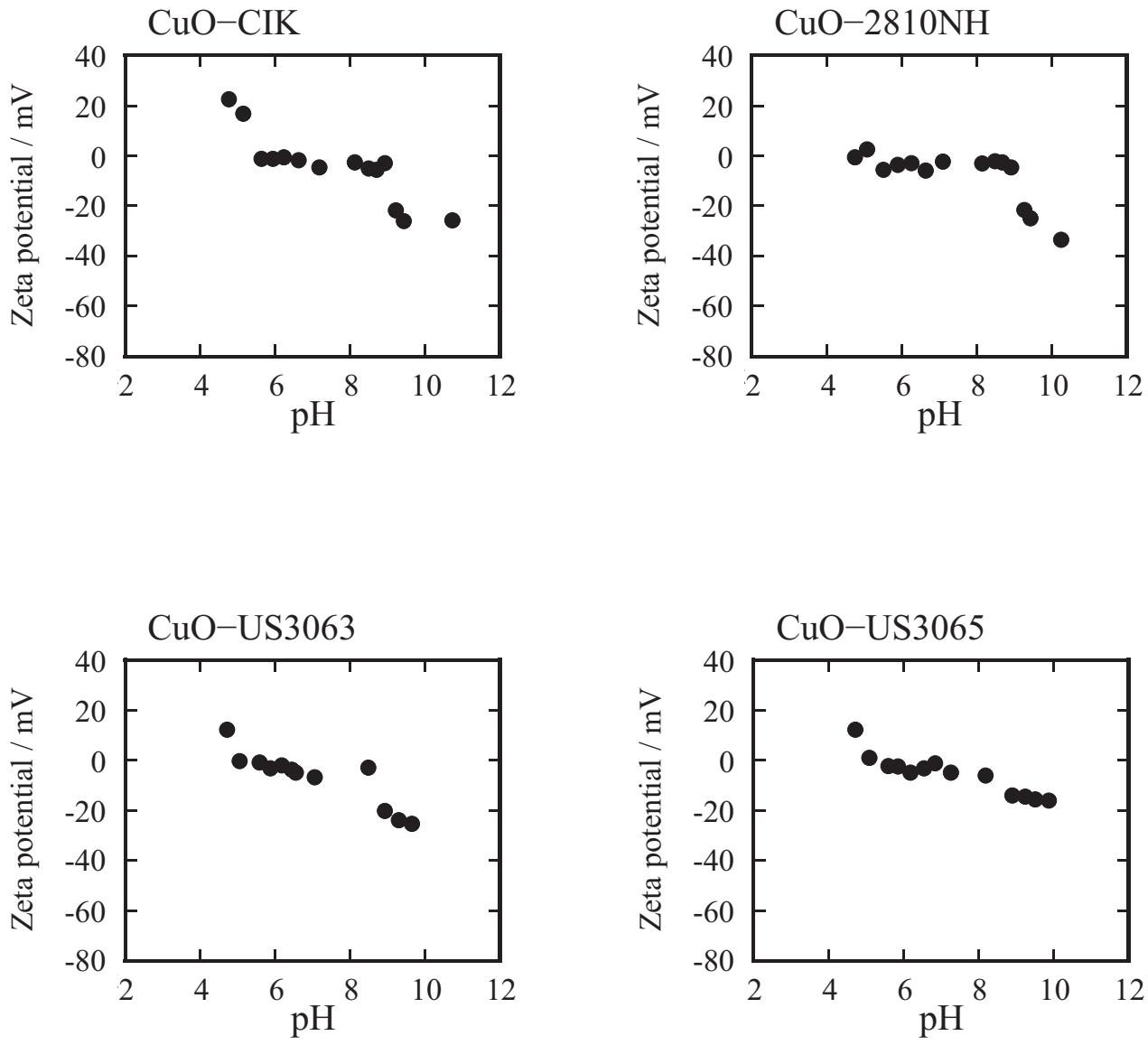

Fig. 9. Plots of zeta potential for copper oxide nanoparticles dispersed in water as a function of pH.
CIK, US3063, US3065: 200 mg dm^{-3}, 2810NH: 500 mg dm^{-3}; Ionic strength: 0.01.

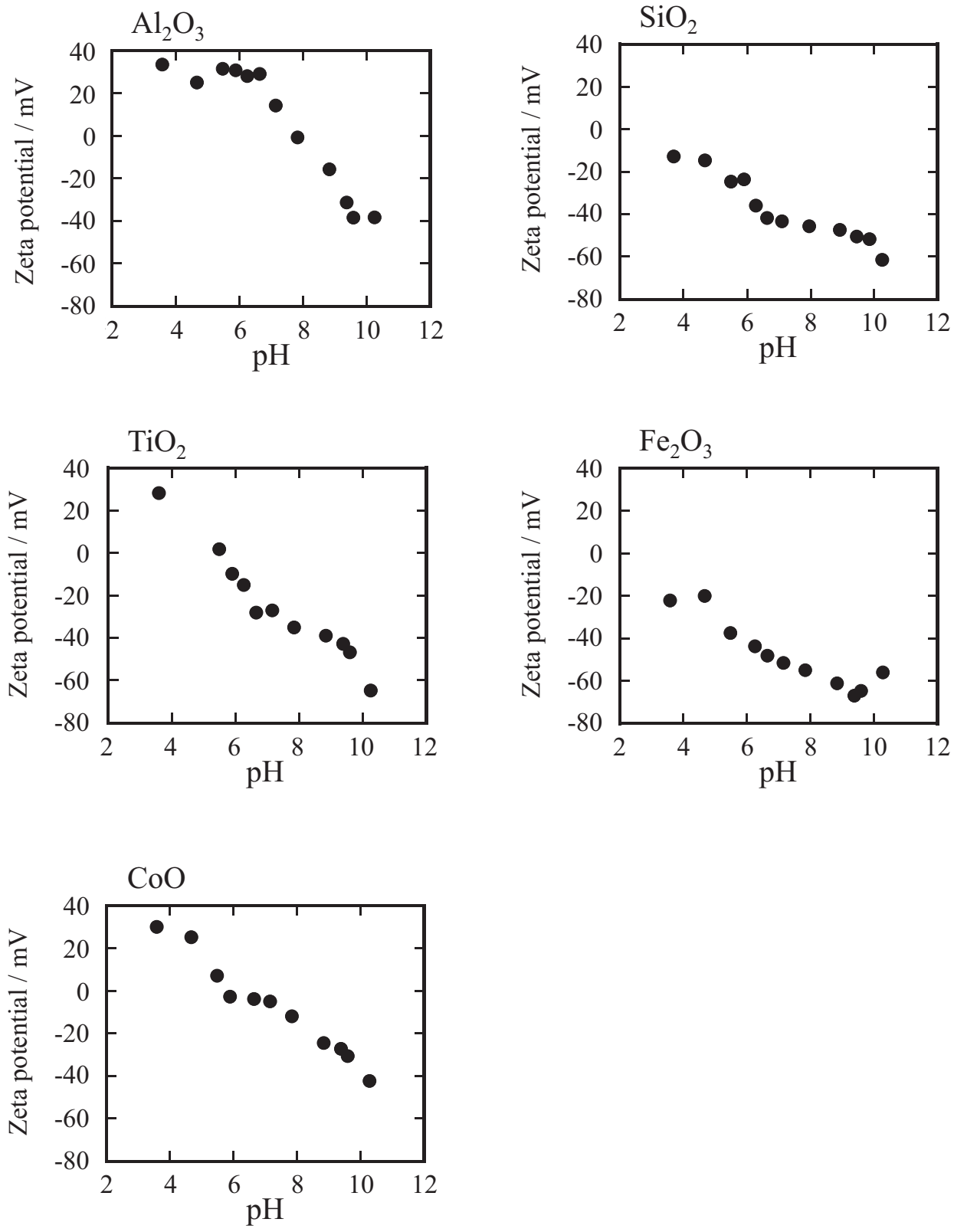

Fig. 10. Plots of zeta potential for metal oxide nanoparticles dispersed in water as a function of pH. Al_2O_3: 100 mg dm^{-3}, SiO_2, TiO_2, Fe_2O_3: 200 mg dm^{-3}, CoO: 180 mg dm^{-3}; Ionic strength: 0.01.

3-4 Particle size distribution

In Fig. 11, the average particle sizes of the four kinds of CuO nanoparticles are shown as a function of pH at a constant ionic strength of 0.01. The results of other nanoparticles are shown in Fig. 12. All the oxides dispersed in water are 5–100 times greater in the average particle size than those in the dry state, showing some aggregation of the nanoparticles in the solution.

For most of the nanoparticles, the respective particle sizes were nearly constant over the experimental pH range (pH 3.7–6.5). In case of TiO_2, CoO, and CuO–CIK, the average particle diameter change is 2–3 times. Although some nanoparticles show size change with the pH as shown in Figs.11 and 12, the trend of D is similar for all the nanoparticles (Figs. 3, 5, and 6). Therefore, it appears that the average particle diameter of the oxide nanoparticles is not a dominant factor determining the distribution ratio of the metal ion.

3-5 Analysis of complexation equilibria on metal oxide nanoparticles surface

3-5-1 Derivation of analytical expression and determination of complexation constant

The hydrolysis constants (K_1 and β_2) of a divalent metal ion (M^{2+}) in an aqueous phase are defined as follows:

$$K_1 = [M(OH)^+][H^+] / [M^{2+}], \quad (7)$$

$$\beta_2 = [M(OH)_2][H^+]^2 / [M^{2+}]. \quad (8)$$

The precipitation reaction and solubility product in aqueous solution phase can be expressed as follows:

$$M^{2+} + 2OH^- \rightleftarrows M(OH)_2\,(\text{solid}), \quad (9)$$

$$K_{sp} = [M^{2+}][OH^-]^2. \quad (10)$$

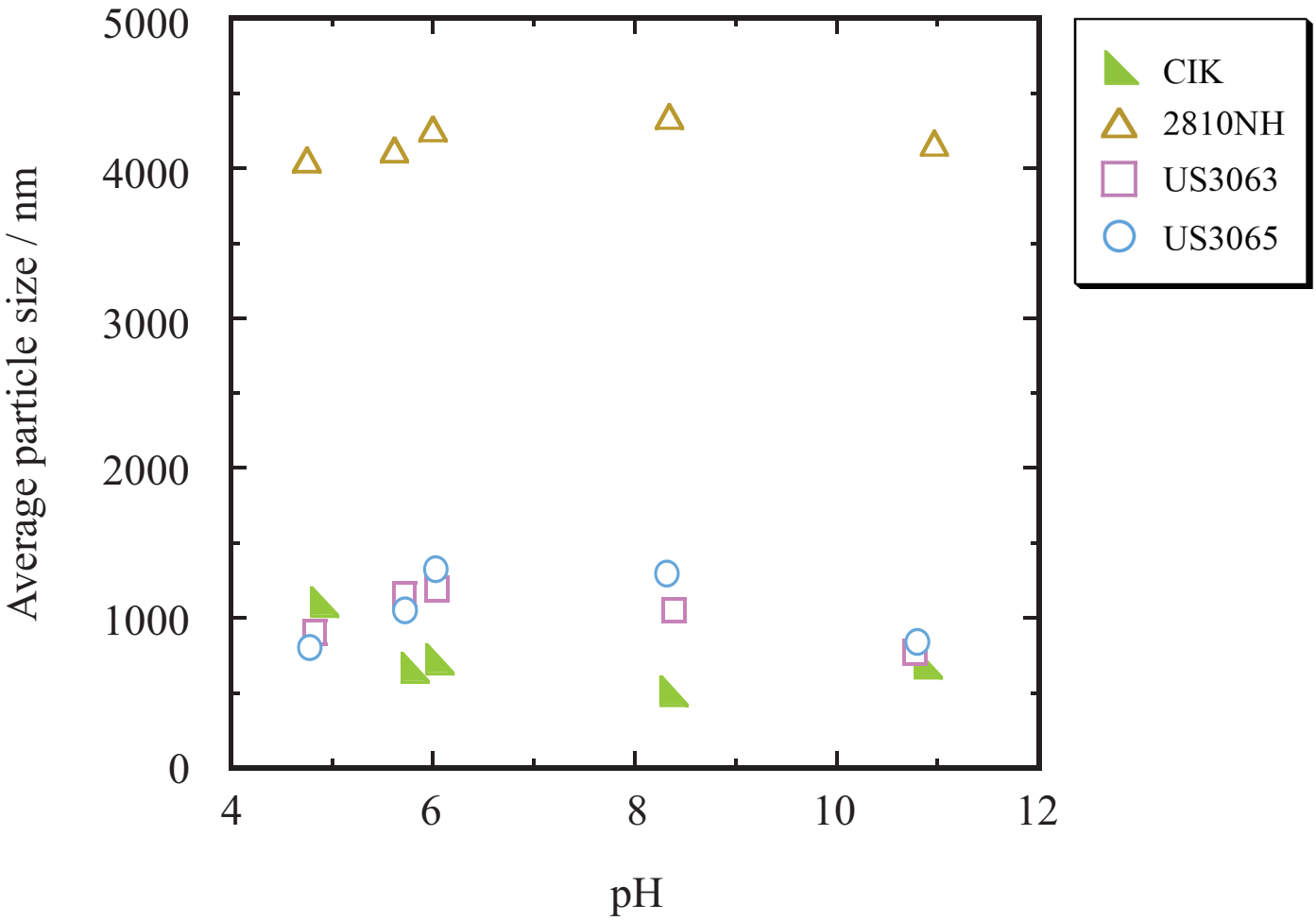

Fig. 11. Plots of average particle size of various copper oxide nanoparticles dispersed in water as a function of pH. Nanoparticles: 1000 mg dm^{-3}; Ionic strength: 0.01.

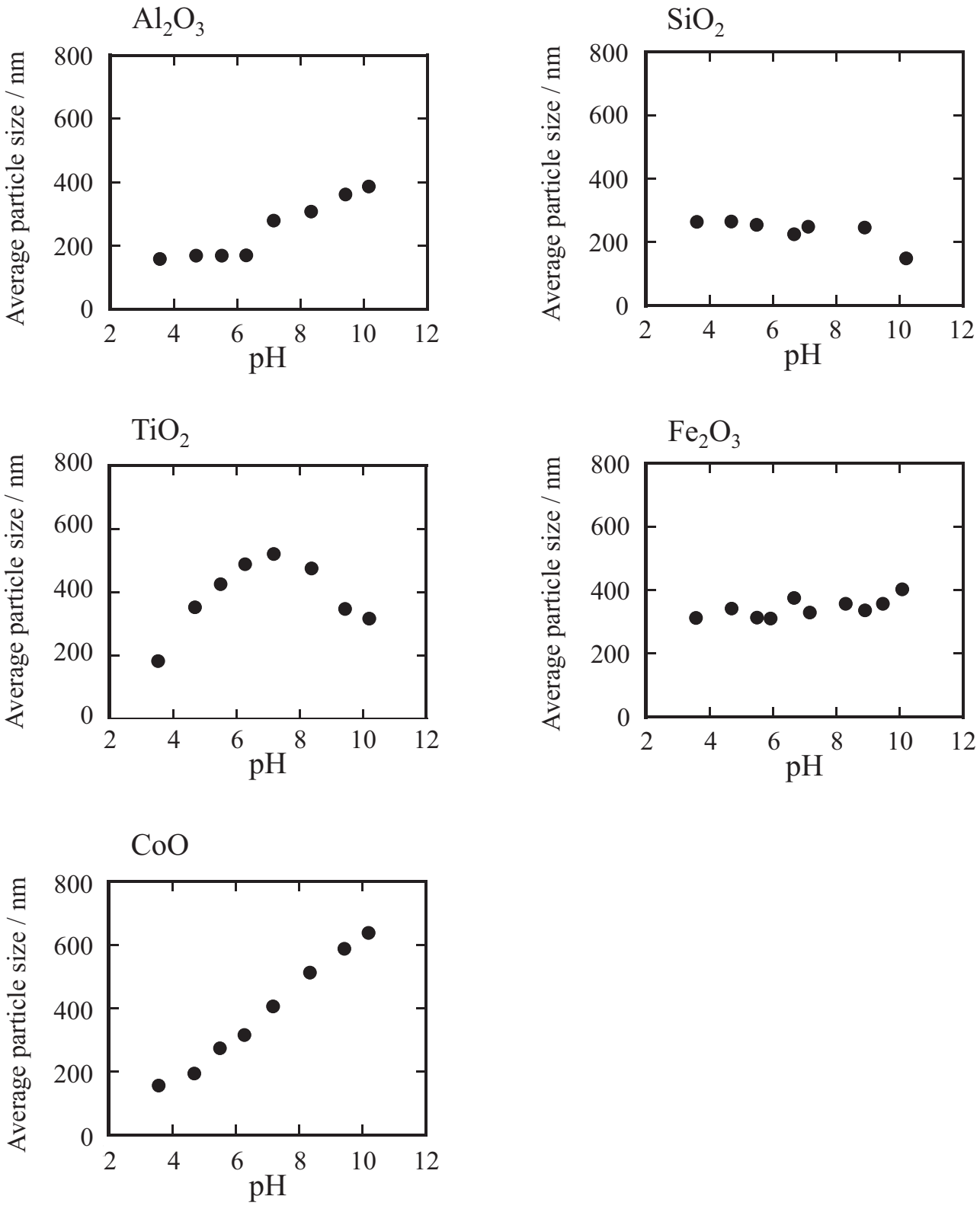

Fig. 12. Plots of average particle size of metal oxide nanoparticles dispersed in water as a function of pH. Al_2O_3: 100 mg dm^{-3}, SiO_2: 150 mg dm^{-3}, TiO_2: 25 mg dm^{-3}, Fe_2O_3, CoO: 60 mg dm^{-3}; Ionic strength: 0.01.

For Be(II), Ni(II), and Cu(II), the values of K_1, β_2, and K_{sp} are summarized in Table 3.[32-34] From the value of K_{sp}, in all cases the metal ions, precipitation of the hydroxide is not generated in the pH conditions of this study.

From Eqs. (7) and (8), the abundance ratio of soluble Be(II) species was calculated as a function of pH as shown in Fig. 13. In the pH range of the present experimental conditions (pH 4–6), the main aqueous species of Be(II) are Be^{2+}, $Be(OH)^{+}$, and Be(OH). In the same way, the abundance of soluble Ni(II) species and Cu(II) were calculated as a function of pH as shown in Figs. 14 and 15, respectively. In the pH range (pH 5–6), the main aqueous species of Ni(II) are Ni^{2+} and $Ni(OH)^{+}$ and that of Cu(II) are Cu^{2+}, $Cu(OH)^{+}$, and $Cu(OH)_2$, respectively. It is expected that the aqueous species having a large valence are favorable to the complexation with the nanoparticles. So, in the following discussion, it is assumed that the divalent ion (Be^{2+}, Ni^{2+}, and Cu^{2+}) is mainly concerned with the surface complexation.

The partition of the metal ion to the metal oxides was evaluated based on the surface complexation model, in which the surface hydroxyl sites on the oxides deprotonate and form complexes with the metal ion in water. The complexation equilibrium can be written as follows:

$$n{>}\text{S-OH} + M^{2+} \quad \rightleftarrows \quad (>\text{S-O})_n M^{(2-n)+} + nH^{+}. \tag{11}$$

The surface complexation constants ($\beta_{S,n}$) are defined by Eq. (12):

$$\beta_{S,n} = [(>\text{S-O})_n M^{(2-n)+}]_S \, [H^{+}]^n / [>\text{S-OH}]_S^{\,n} \, [M^{2+}]. \tag{12}$$

Here, [X] and $[X]_S$ denote the concentration of a material X in the aqueous phase (mol dm^{-3}) and that in the nanoparticle phase (mol g^{-1}), respectively. The symbol n represents the number of the surface $-O^{-}$ groups bound to a metal ion. The general coordination number is 4, 6, and 6 for Be(II), Ni(II), and Cu(II), respectively.[35] Considering the coordination number, the value of n can be taken to be 1–4, 1–6, and 1–6 for Be(II), Ni(II), and Cu(II), respectively. The concentration of $(>\text{S-O})_n M^{(2-n)+}$ on

Table 3. Hydrolysis constants and solubility product constants of the metal ion in the water

	Hydrolysis constants		Solubility product constants
	$\log K_1$	$\log \beta_2$	$\log K_{sp}$
Be(II)	−5.7	−11.68	−21.3
Ni(II)	−9.6	−19.0	−19.3
Cu(II)	−7.95	−16.2	−14.7

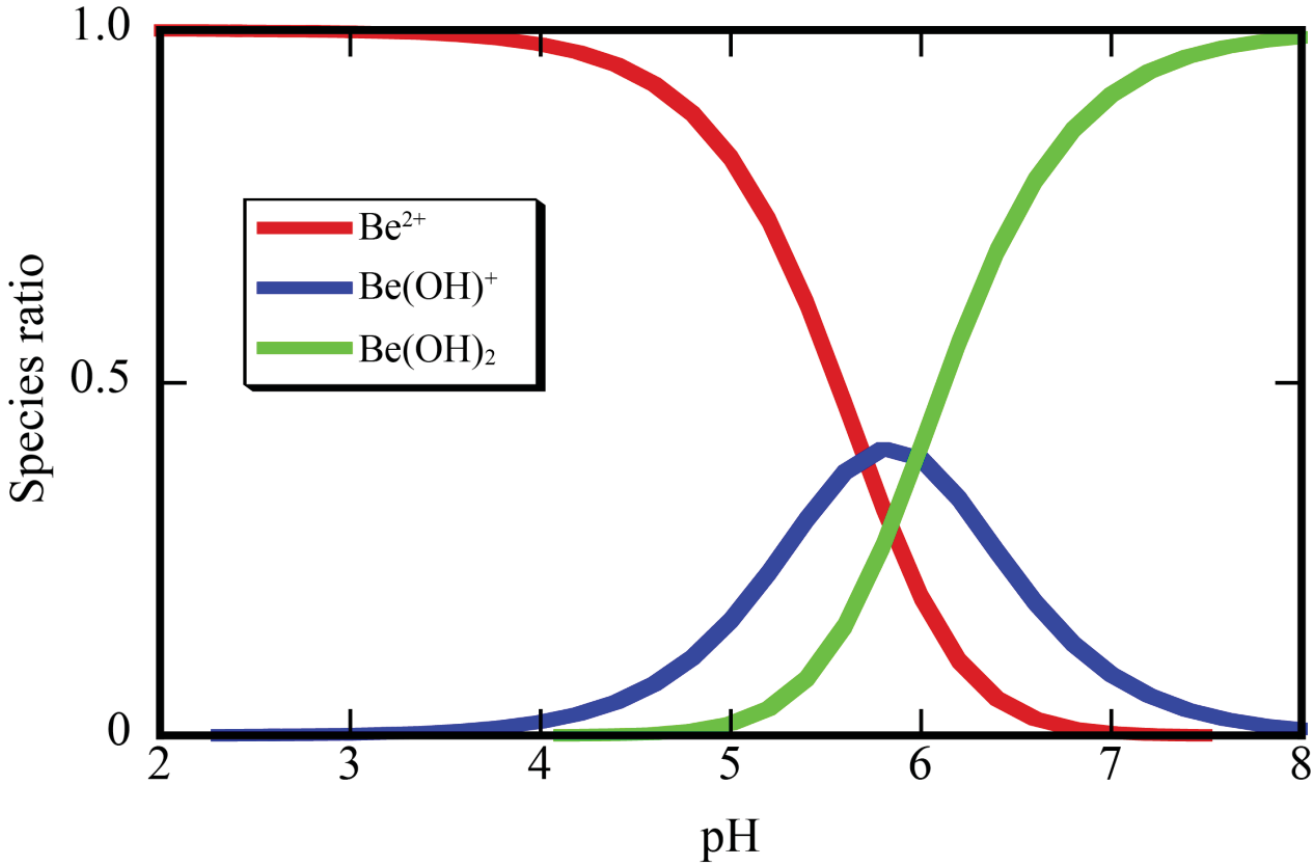

Fig. 13. Calculation of soluble Be(II) species in water as a function of pH.

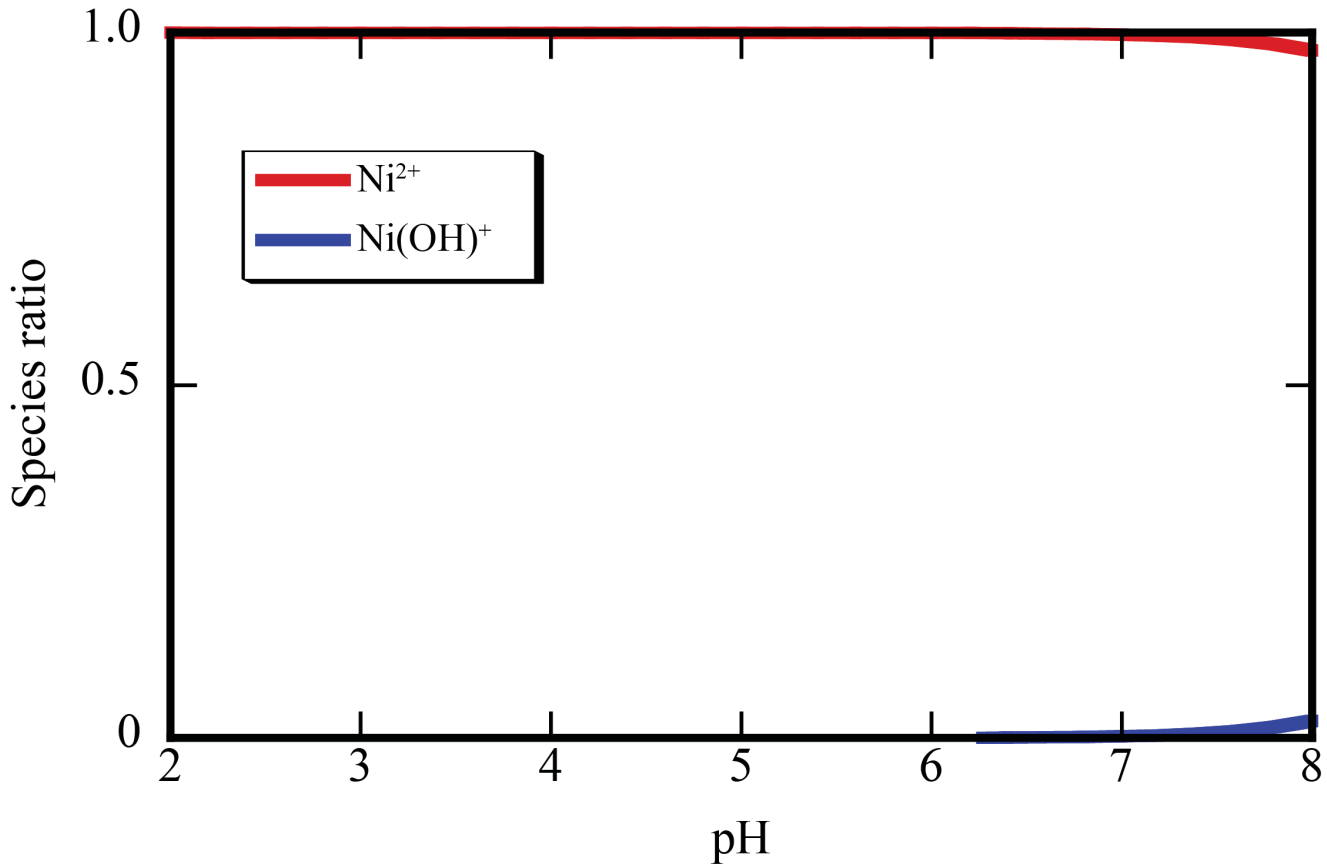

Fig. 14. Calculation of soluble Ni(II) species in water as a function of pH.

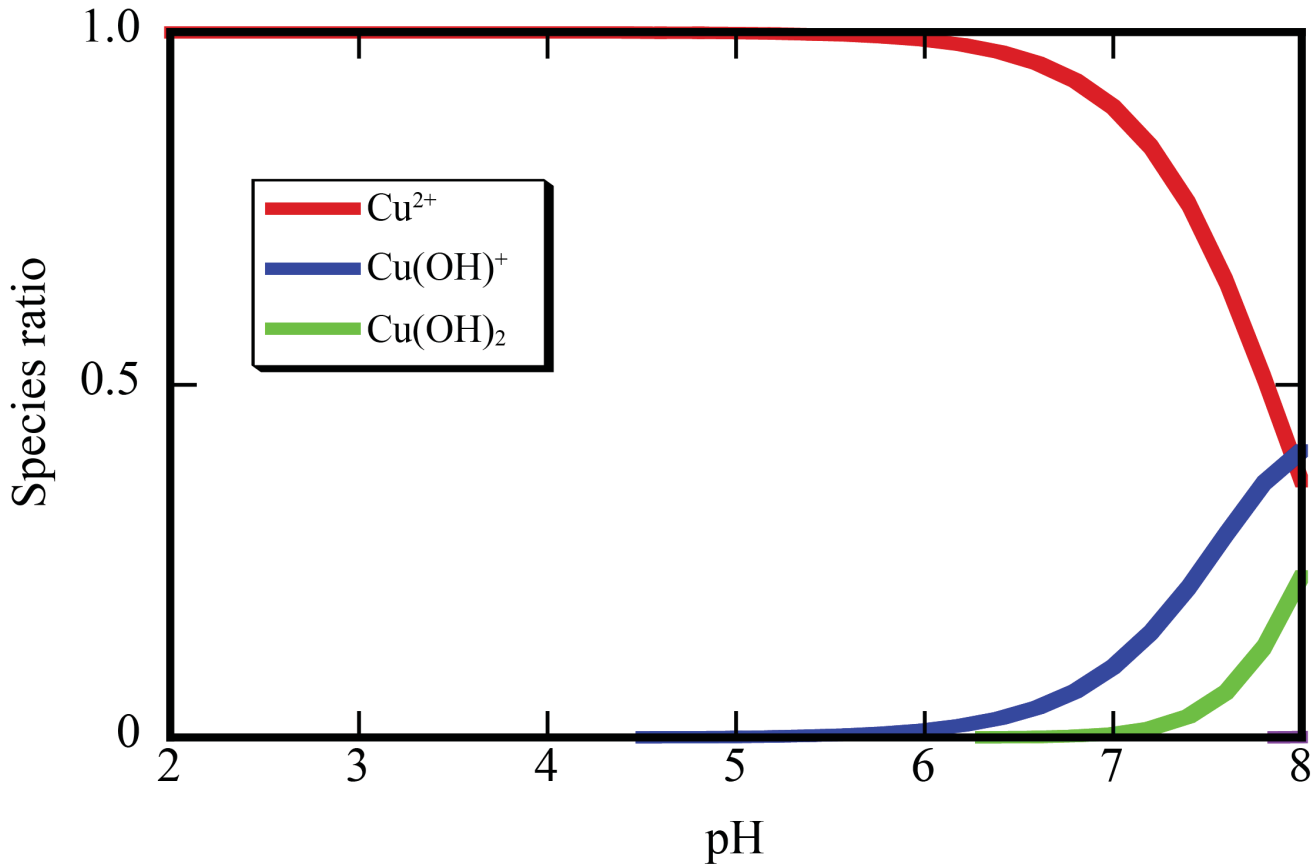

Fig. 15. Calculation of soluble Cu(II) species in water as a function of pH.

the oxide nanoparticles is written as follows:

$$[(>\text{S-O})_n\text{M}^{(2-n)+}]_\text{S} = [\text{M}^{2+}]\{\beta_{\text{S},n}\,[>\text{S-OH}]_\text{S}^{\,n}[\text{M}^{2+}] / [\text{H}^+]^n\}. \quad (13)$$

The total concentrations of the metal ion in the aqueous solution phase are calculated using Eqs. (7) and (8) as follows:

$$[\text{M}^{2+}] + [\text{M(OH)}^+] + [\text{M(OH)}_2] = [\text{M}^{2+}](1 + K_1 / [\text{H}^+] + \beta_2 / [\text{H}^+]^2). \quad (14)$$

From Eqs. (13) and (14), D is expressed as follows:

$$D = \sum_n [(>\text{S-O})_n\text{M}^{(2-n)+}]_\text{S} / ([\text{M}^{2+}] + [\text{M(OH)}^+] + [\text{M(OH)}_2])$$

$$= \sum_n \{\beta_{\text{S},n}\,[>\text{S-OH}]_\text{S}^{\,n} / [\text{H}^+]^n / (1 + K_1 / [\text{H}^+] + \beta_2 / [\text{H}^+]^2)\}. \quad (15)$$

The following equation is derived from Eq. (15):

$$\log D + \log (1 + K_1 / [\text{H}^+] + \beta_2 / [\text{H}^+]^2) = \sum_n \log \{\beta_{\text{S},n}\,[>\text{S-OH}]_\text{S}^{\,n} / [\text{H}^+]^n\}. \quad (16)$$

In the case where n takes a single value, Eq. (16) is expressed as follows:

$$\log D + \log (1 + K_1 / [\text{H}^+] + \beta_2 / [\text{H}^+]^2) = \log \beta_{\text{S},n} + n \log [>\text{S-OH}]_\text{S} + n\,\text{pH}. \quad (17)$$

The left-hand-side of Eq. (17) calculated are plotted versus pH as shown in Figs. 16 (Be(II)), 17 (Ni(II)), and 18 (Cu(II)). In Figs. 16–18, the slopes of the lines indicate the

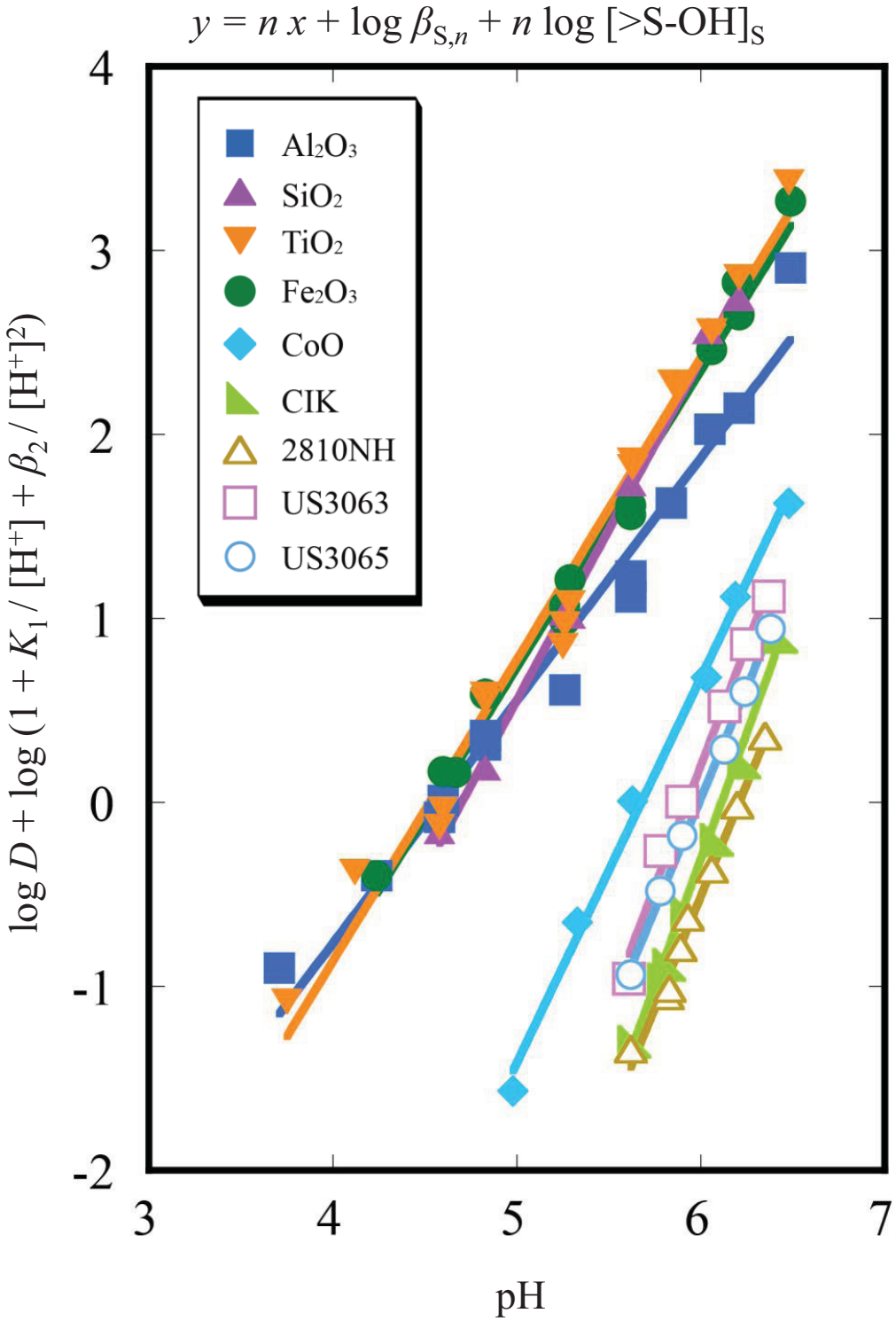

Fig. 16. Plots of [log D + log (1 + K_1 / [H$^+$] + β_2 / [H$^+$]^2)] for the distribution of Be(II) on metal oxide nanoparticles in water as a function of pH. The lines denote the linear least-squares fitting results according to Eq. (17).

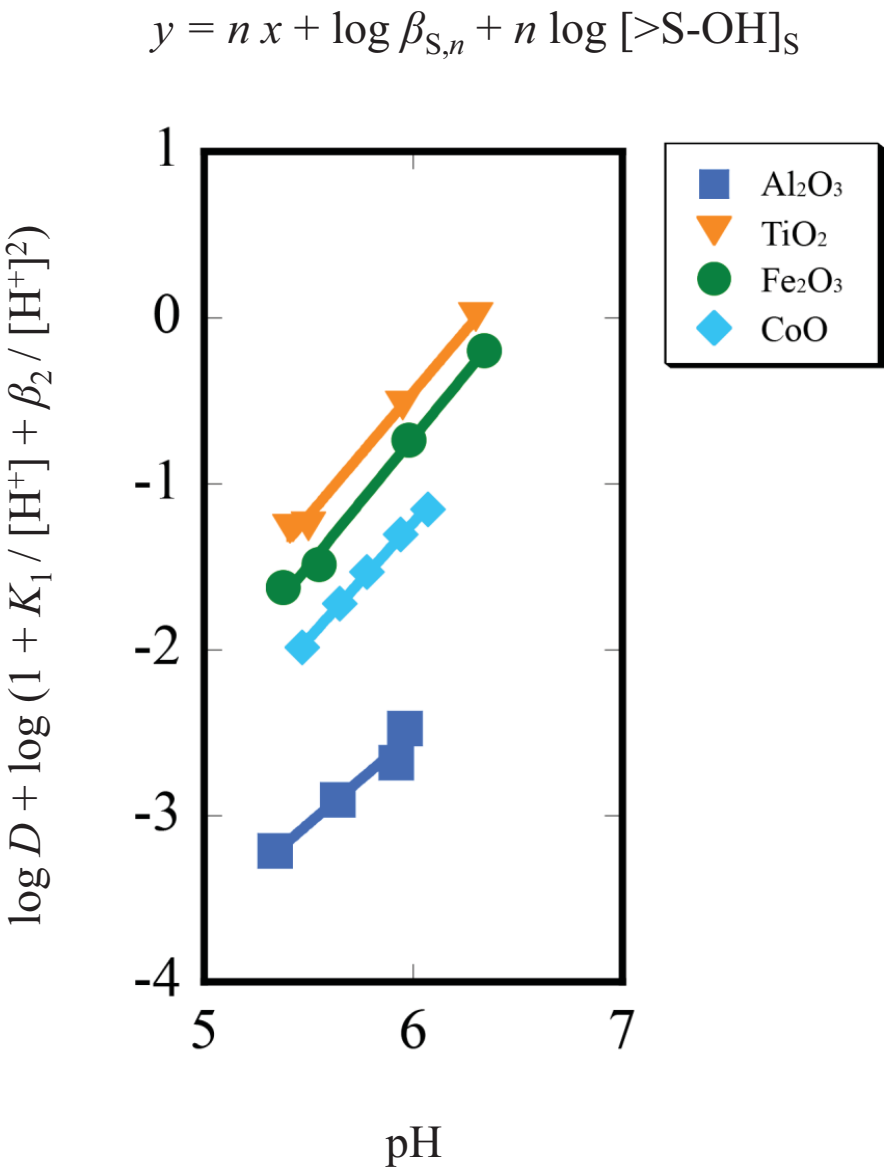

Fig. 17. Plots of [log D + log (1 + K_1 / [H$^+$] + β_2 / [H$^+$]^2)] for the distribution of Ni(II) on metal oxide nanoparticles in water as a function of pH. The lines denote the linear least-squares fitting results according to Eq. (17).

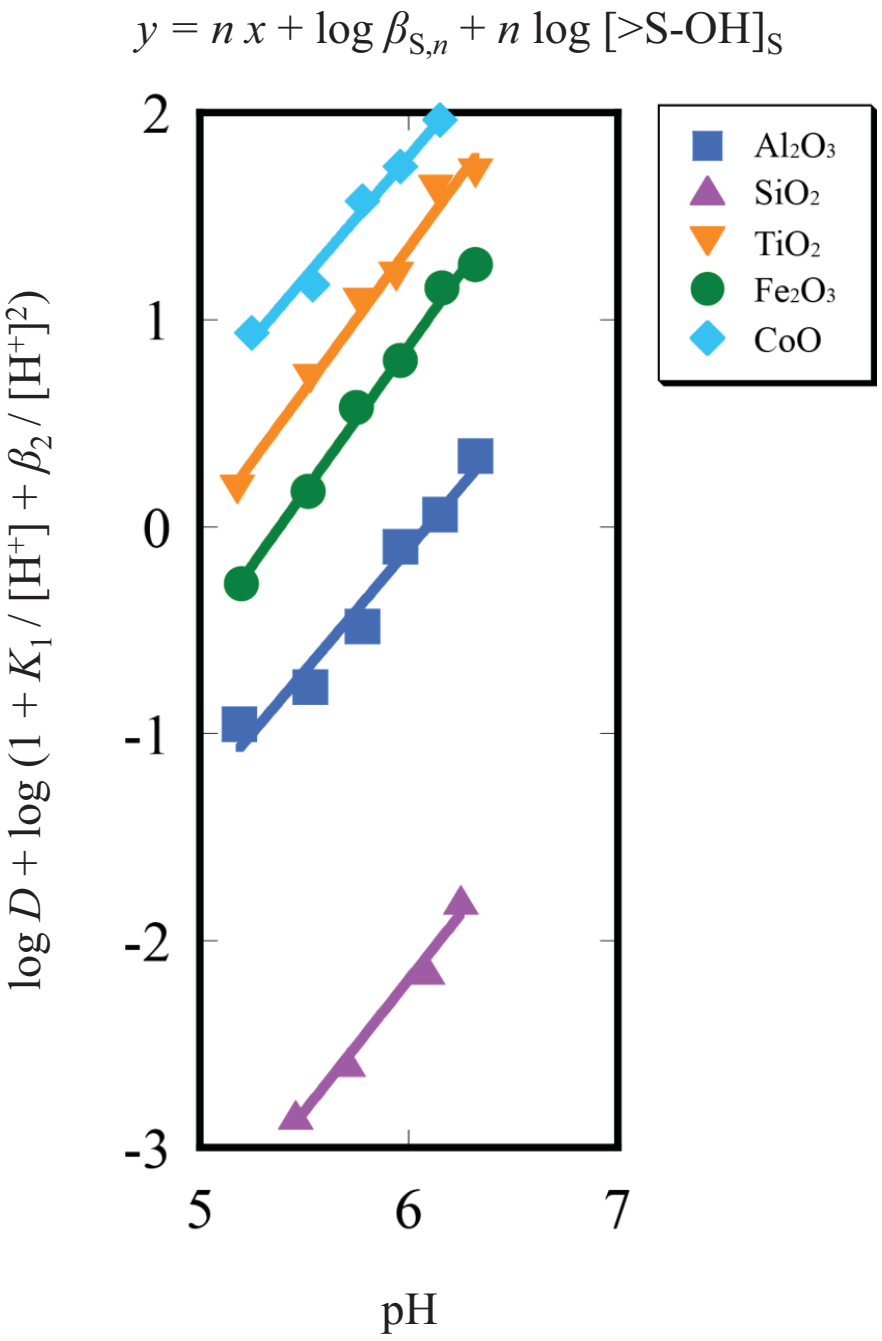

Fig. 18. Plots of [log D + log (1 + K_1 / [H$^+$] + β_2 / [H$^+$]^2)] for the distribution of Cu(II) on metal oxide nanoparticles in water as a function of pH. The lines denote the linear least-squares fitting results according to Eq. (17).

n values. The slope and intercept values of the lines are summarized in Table 4.

For most of the systems, the slope value is between 1 and 2; this suggests that $n = 1$ and 2. These slope values imply that two kinds of complexes, $(>S\text{-}O)M^+$ and $(>S\text{-}O)_2M$, are the dominant M(II) species formed on the surface of the oxide nanoparticles. Herein, Eq. (16) can be simplified as Eq. (18):

$$\log D + \log (1 + K_1 / [H^+] + \beta_2 / [H^+]^2) = \log (\beta_{S,1}[>S\text{-}OH]_S / [H^+] + \beta_{S,2}[>S\text{-}OH]_S^2 / [H^+]^2). \quad (18)$$

On the other hand, for the partition of Be(II) onto CoO, CuO–CIK, CuO–2810NH, CuO–US3063, and CuO–US3065, the slope is between 2 and 3; this suggests that $n = 2$ and 3. These slope values imply that two kinds of complexes, $(>S\text{-}O)_2Be$, and $(>S\text{-}O)_3Be^-$, are the dominant Be(II) species formed on the surface of the oxide nanoparticles. Herein, Eq. (16) can be simplified as Eq. (19):

$$\log D + \log (1 + K_1 / [H^+] + \beta_2 / [H^+]^2) = \log (\beta_{S,2}[>S\text{-}OH]_S^2 / [H^+]^2 + \beta_{S,3}[>S\text{-}OH]_S^3 / [H^+]^3). \quad (19)$$

Using the surface hydroxyl site concentrations ($[>S\text{-}OH]_S$) shown in Table 2, the values of $\beta_{S,1}$, $\beta_{S,2}$, and $\beta_{S,3}$ were obtained by nonlinear least-squares fitting according to Eqs. (18) or (19). The lines are the regression curves and fit well the experimental data as shown in Figs. 19 (Be(II)), 20 (Ni(II)), and 21 (Cu(II)). The $\beta_{S,n}$ values are summarized in Table 5.

3-5-2 Difference of complexation constant depending on type of CuO nanoparticles

In this section, the $\beta_{S,n}$ values of Be(II) for four types of CuO nanoparticles are compared. The $\beta_{S,2}$ values are similar for all four kinds of CuO nanoparticles. As shown in Fig. 11, the average particle sizes dispersed in water are different depending on the kind of CuO nanoparticles; thus the similarity in the $\beta_{S,2}$ values for the different CuO

Table 4. Regression slopes and intercepts for metal oxide nanoparticles*

	Be(II)		Ni(II)		Cu(II)	
	Slopes	Intercepts	Slopes	Intercepts	Slopes	Intercepts
Al_2O_3	1.32	−6.04	1.07	−8.94	1.19	−7.24
SiO_2	1.85	−8.70			1.28	−9.84
TiO_2	1.64	−7.42	1.49	−9.36	1.38	−6.93
Fe_2O_3	1.61	−7.33	1.54	−9.95	1.41	−7.61
CoO	2.18	−12.4	1.34	−9.27	1.18	−5.29
CuO−CIK	2.74	−16.8				
CuO−2810NH	2.44	−15.1				
CuO−US3063	2.50	−14.8				
CuO−US3065	2.42	−14.5				

* Calculated from the date in Figs. 16, 17, and 18 according to Eq. (17).

Al_2O_3, SiO_2, TiO_2, Fe_2O_3:

$$y = \log (\beta_{S,1}[\text{>S-OH}]_S / 10^{-x} + \beta_{S,2}[\text{>S-OH}]_S^2 / 10^{-2x})$$

CoO, CuO−CIK, CuO−2810NH, CuO−US3063, CuO−US3065:

$$y = \log (\beta_{S,2}[\text{>S-OH}]_S^2 / 10^{-2x} + \beta_{S,3}[\text{>S-OH}]_S^3 / 10^{-3x})$$

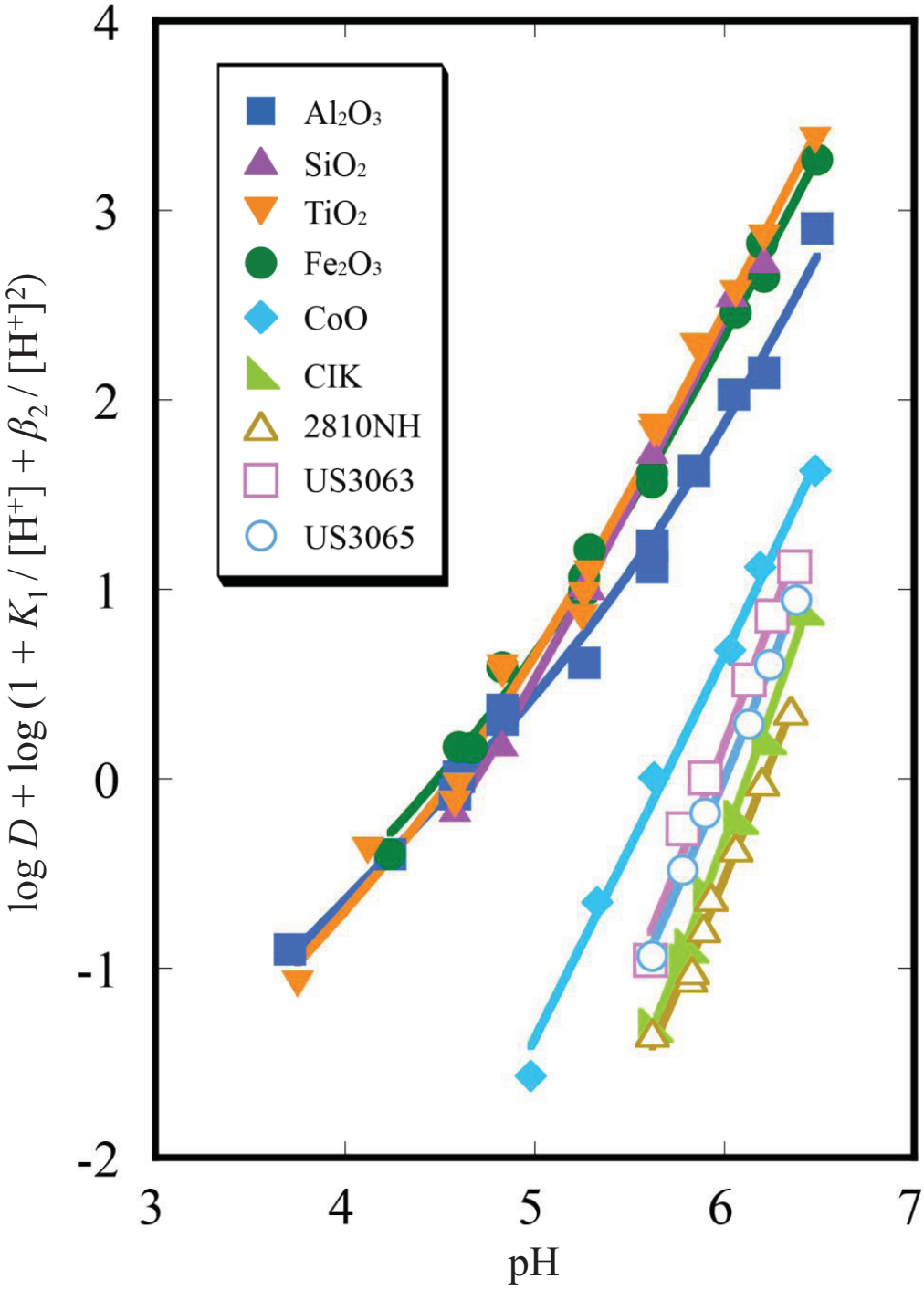

Fig. 19. Plots of [log D + log (1 + K_1 / [H^+] + β_2 / [H^+]^2)] for the distribution of Be(II) on metal oxide nanoparticles in water as a function of pH. The lines denote the nonlinear least-squares fitting results according to Eq. (18) for Al_2O_3, SiO_2, TiO_2, Fe_2O_3 and Eq. (19) for CoO, CuO−CIK, CuO−2810NH, CuO−US3063, CuO−US3065.

$$y = \log (\beta_{S,1}[>\text{S-OH}]_S / 10^{-x} + \beta_{S,2}[>\text{S-OH}]_S^2 / 10^{-2x})$$

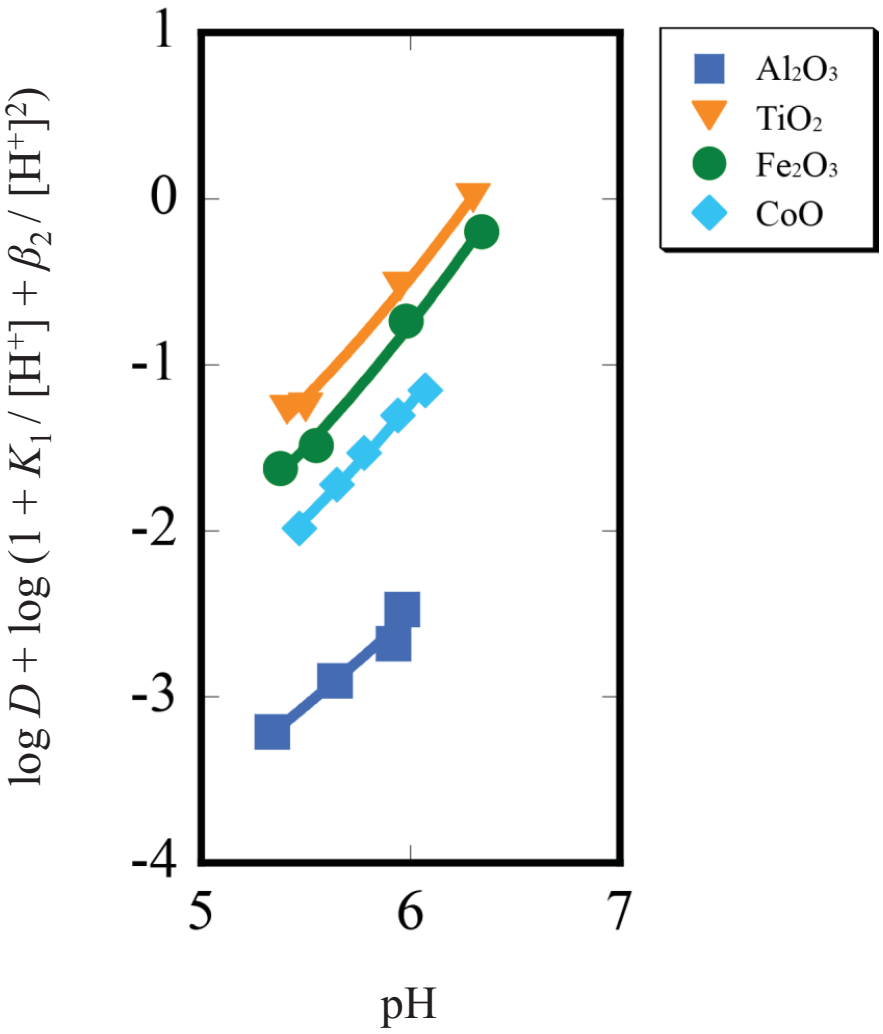

Fig. 20. Plots of [log D + log (1 + K_1 / [H$^+$] + β_2 / [H$^+$]^2)] for the distribution of Ni(II) on metal oxide nanoparticles in water as a function of pH. The lines denote the nonlinear least-squares fitting results according to Eq. (18).

$$y = \log (\beta_{S,1}[\text{>S-OH}]_S / 10^{-x} + \beta_{S,2}[\text{>S-OH}]_S^2 / 10^{-2x})$$

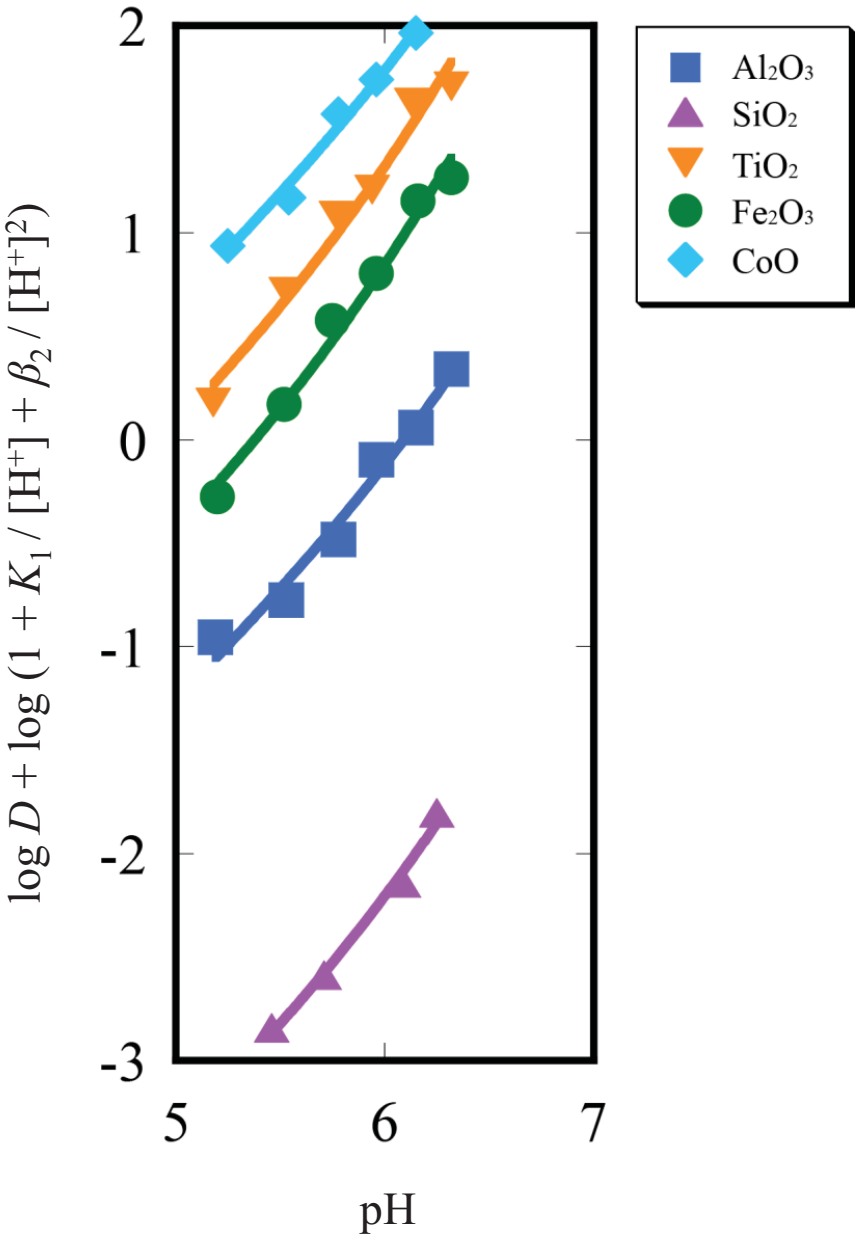

Fig. 21. Plots of [log D + log (1 + K_1 / [H$^+$] + β_2 / [H$^+$]^2)] for the distribution of Cu(II) on metal oxide nanoparticles in water as a function of pH. The lines denote the nonlinear least-squares fitting results according to Eq. (18).

Table 5. Surface complexation constants of Be(II), Ni(II), and Cu(II) with metal oxide nanoparticles in water ($\beta_{S,1}$, $\beta_{S,2}$, and $\beta_{S,3}$)

	Be(II)			Ni(II)		Cu(II)	
	$\log \beta_{S,1}$	$\log \beta_{S,2}$	$\log \beta_{S,3}$	$\log \beta_{S,1}$	$\log \beta_{S,2}$	$\log \beta_{S,1}$	$\log \beta_{S,2}$
Al_2O_3	−0.69±0.04	−2.35±0.06		−4.61±0.10	−7.39±0.87	−2.31±0.08	−4.72±0.20
SiO_2	−1.17±0.14	−1.71±0.04				−4.45±0.07	−6.79±0.15
TiO_2	−0.62±0.09	−1.28±0.05		−2.71±0.07	−4.44±0.08	−0.83±0.10	−2.71±0.14
Fe_2O_3	−0.27±0.06	−1.10±0.04		−2.87±0.08	−4.34±0.08	−1.17±0.08	−2.81±0.10
CoO		−3.99±0.08	−6.92±0.38	−3.81±0.04	−6.04±0.07	−0.62±0.05	−3.28±0.19
CuO−CIK		−4.03±0.12	−5.17±0.05				
CuO−2810NH		−3.82±0.09	−5.44±0.11				
CuO−US3063		−4.36±0.22	−6.13±0.13				
CuO−US3065		−4.03±0.06	−6.10±0.08				

nanoparticles implies that the stability of $(>S\text{-}O)_2Be$ complexes is not largely affected by the particle size. On the other hand, the $\beta_{S,3}$ values vary with the kind of CuO nanoparticles. The differences in $\beta_{S,3}$ may be related with the structure or conformation of the surface hydroxyl sites on the CuO nanoparticles. Both the $\beta_{S,2}$ and $\beta_{S,3}$ values are similar for CuO–US3063 and CuO–US3065 which were prepared by the same manufacturer.

The dependence of the complexation constants on the kind of CuO nanoparticles can not be clearly explained at the present stage. More comprehensive investigations for characterizing the nanoparticles by physical / chemical analytical techniques and microscopic observations would be valuable for clarifying the characteristic surface complexation properties for each CuO nanoparticles.

3-5-3 Difference of complexation constant depending on metal ions

In this section, the differences of the $\beta_{S,n}$ values among the metal ions are discussed. It is known that the metal ion having a large hydrolysis constant is favorable to the complexation with a metal oxide.[19] In Fig. 22, the log $\beta_{S,n}$ plotted versus the logarithmic values of the hydrolysis constants for metal ions. Except for CoO, the $\beta_{S,n}$ value increases with an increase of the hydrolysis constant. In other words, the reaction of the metal ion to the surface hydroxyl sites on the nanoparticle is similar to the hydrolysis reaction of the metal ion. This result supports the surface hydroxyl sites are concerned with the complexation of the metal ions on the oxide nanoparticles.

3-5-4 Difference of complexation constant depending on kind of oxide nanoparticles

In this section, the differences among the metal oxides of the $\beta_{S,n}$ values are discussed.

In the partition behavior of Be(II) to the oxide nanoparticles, the $\beta_{S,1}$, $\beta_{S,2}$, and $\beta_{S,3}$ values decrease in the order, $Fe_2O_3 > TiO_2 \approx Al_2O_3 > SiO_2$ ($\beta_{S,1}$), $Fe_2O_3 > TiO_2 > SiO_2 > Al_2O_3 >> CoO \approx$ CuO–CIK ($\beta_{S,2}$), and CuO–CIK > CoO ($\beta_{S,3}$), respectively. It is expected that the oxide having a positive zeta potential is unfavorable to the

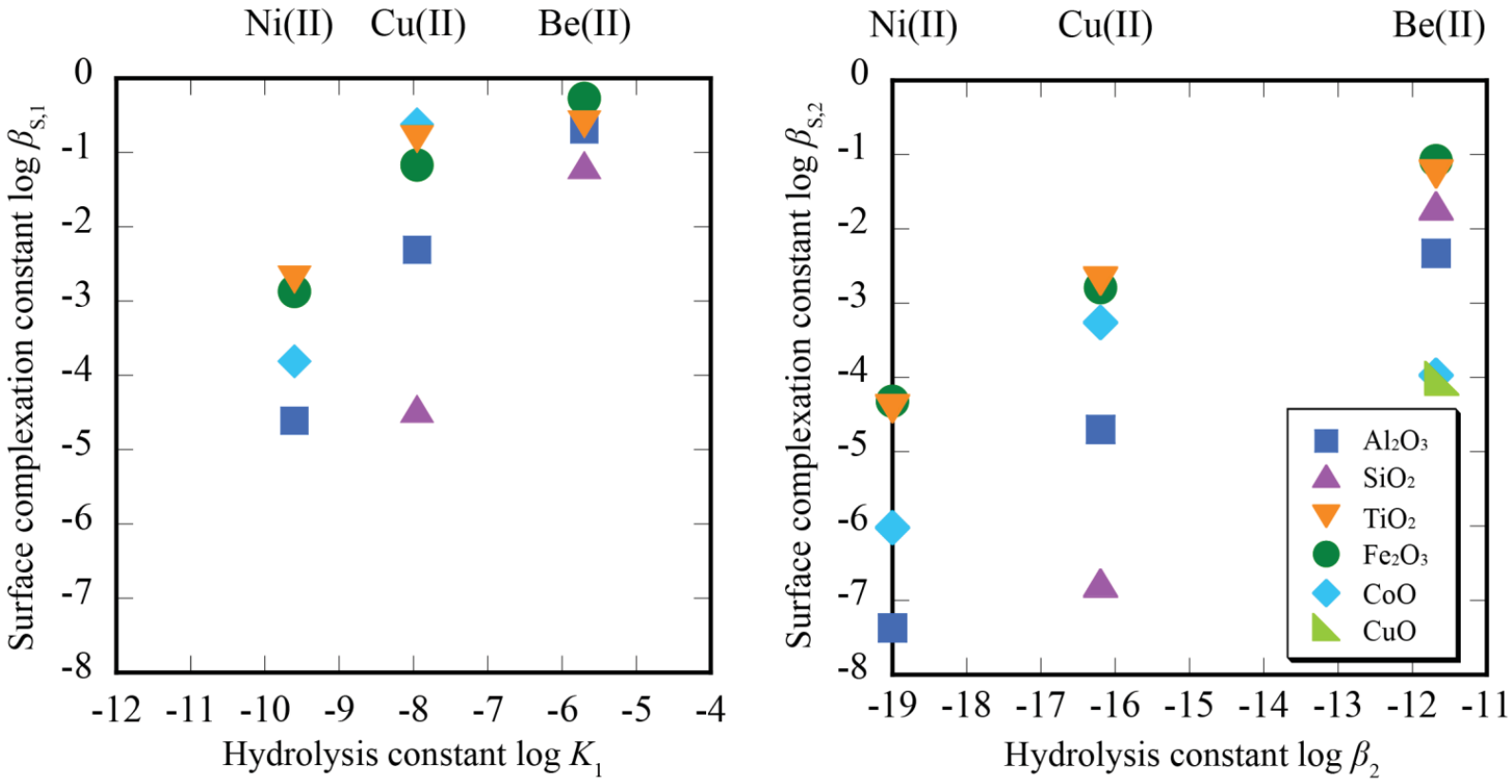

Fig. 22. Plots of surface complexation constants with some metal oxides versus the hydrolysis constants for metal ions.
Left side figure shows the data for complexation between one metal ion and one >S-O$^-$ or OH$^-$.
Right side figure shows the data for complexation between one metal ion and two >S-O$^-$ or OH$^-$.
(CuO: CuO−CIK)

complexation with the Be^{2+} cation. However, Al_2O_3 (positive charged) have a much larger $\beta_{S,2}$ value than CoO and CuO–CIK (nearly neutral). In addition, when the *n* value is 2, the surface charge of the nanoparticles does not change before and after the complexation reaction (Eq. (11)). Therefore, it appears that the zeta potential of the oxide nanoparticles is not a dominant factor determining their reactivity for Be^{2+}. The same holds true for Ni^{2+} and Cu^{2+}.

Although the complexation ability of CoO and CuO–CIK is smaller as compared to that of other oxides, only CoO and CuO–CIK form $(>S\text{-}O)_3Be^-$ complexes on the surface. In order that three $>S\text{-}O^-$ can bind to a Be^{2+} ion, a close positioning of the hydroxyl sites is necessary. So the surface hydroxyl site density (the amount of hydroxyl sites per unit area of the surface) was evaluated under some assumptions. Assuming that the nanoparticles in water comprise a hexagonal close-packed array of uniform spherical particles which have a diameter equal to the average particle size of the dry nanoparticles, the packing efficiency of the spheres is 0.74. By considering the packing efficiency, the surface hydroxyl site density can be estimated from the data in Table 1. The densities (unit: mol m^{-2}) are 8×10^{-6}, 8×10^{-6}, 1×10^{-5}, 1×10^{-5}, 3×10^{-5}, and 2×10^{-5} for Al_2O_3, SiO_2, TiO_2, Fe_2O_3, CoO, and CuO–CIK, respectively. These values are comparable, in the order of magnitude, to the literature values.[36] The surface hydroxyl density suggests that the surface hydroxyl sites are more closely positioned on the CoO and CuO–CIK nanoparticles than on other oxides. The density, however, may also depend on the preparation method of the oxide. On the contrary, in the case of Ni(II) and Cu(II), $(>S\text{-}O)_3M^-$ complexes on the surface of CoO and CuO–CIK is not observed. The ionic radii of Ni(II) and Cu(II) is larger than that of Be(II). It is possible that the hydroxyl sites may be too close together for Ni(II) and Cu(II) to bind three hydroxyl sites.

From thermodynamic viewpoint, the complexation reaction of Eq. (11) can be considered to consist of the following two equilibrium processes:

$$>S\text{-}OH \quad \rightleftarrows \quad >S\text{-}O^- + H^+, \tag{20}$$

$$n\text{>S-O}^- + \text{M}^{2+} \quad \rightleftarrows \quad (\text{>S-O})_n\,\text{M}^{(2-n)+}. \qquad (21)$$

Eqs. (20) and (21) show deprotonation of the surface hydroxyl site (>S-OH) and bonding of the negatively charged deprotonated site (>S-O$^-$) to M^{2+}, respectively. The reaction of Eq. (20) should be facilitated with decreasing charge density of the oxygen atom of >S-OH. If the bond between >S-O$^-$ and M^{2+} is governed by an electrostatic interaction, the reaction of Eq. (21) should also depend on the charge density of the oxygen atom of >S-O$^-$; in this case, an increase of the oxygen charge density facilities the reaction of Eq. (21). Therefore, the reaction of Eqs. (20) and (21) are oppositely affected by the charge density of the oxygen atom which should decrease with increasing electronegativity of the metal (or Si) composing the oxide.

Tanaka and Ozaki reported the electronegativity (X_i) of the lattice metal ions of oxide.[37] The X_i is given by the following equation:

$$X_i = (1 + 2Z) X_0, \qquad (22)$$

where Z and X_0 are the valence of the lattice metal ions of oxide and Pauling's electronegativity,[38] respectively. This equation was developed from the relation $X_i = (\partial I / \partial Z)$, where I is the ionization potential of the metals. The X_i values calculated by Eq. (22) were used for evaluating activity of catalyst[39, 40] and Co^{2+} adsorption properties of metal oxide.[41]

For the oxides in this study, the X_i values calculated are as follows: in increasing order of X_i, CoO (X_i = 9.0), CuO (X_i = 9.5), Al_2O_3 (X_i = 10.5), Fe_2O_3 (X_i = 12.6), TiO_2 (X_i = 13.5), and SiO_2 (X_i = 16.2). The log $\beta_{S,n}$ (n = 1, 2, and 3) values are plotted against the X_i value in Figs. 23 (Be(II)), 24 (Ni(II)), and 25 (Cu(II)).

As shown in Fig. 23, the log $\beta_{S,n}$ values of Be(II) increase with an increase of X_i from CoO to Fe_2O_3. This result suggests that the complexation of Be(II) with the oxide nanoparticles (Eq. (11)) is governed by the deprotonation of >S-OH (Eq. (20)) than the bonding of >S-O$^-$ to Be^{2+} (Eq. (21)). A similar result was reported for the complexation of Co^{2+} with metal oxides.[41] However, in the higher X_i region (Fe_2O_3, TiO_2, and SiO_2),

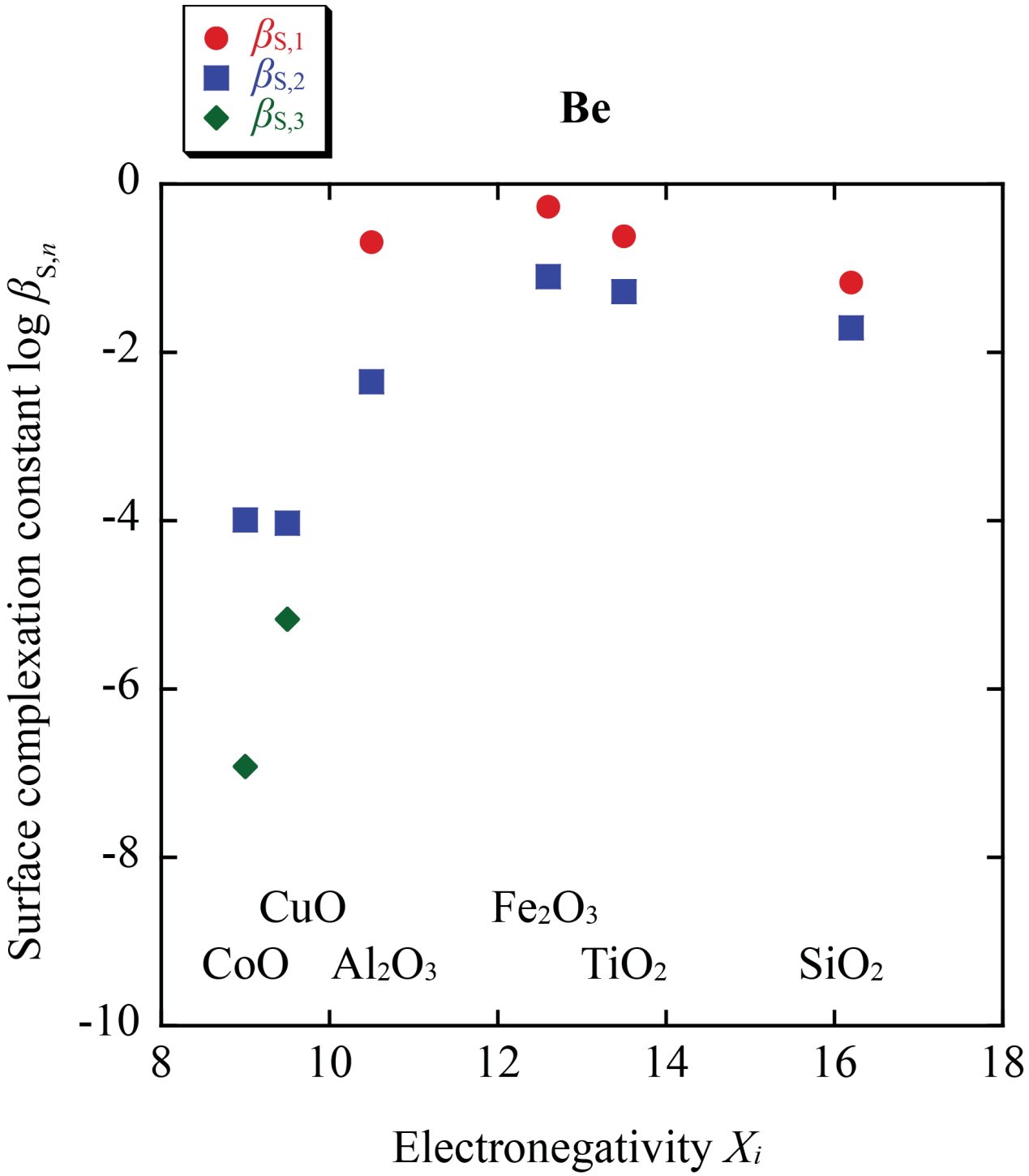

Fig. 23. Plots of surface complexation constants for the distribution of Be(II) on metal oxide nanoparticles in water as a function of X_i for metal oxide nanoparticles according to Eq. (22).

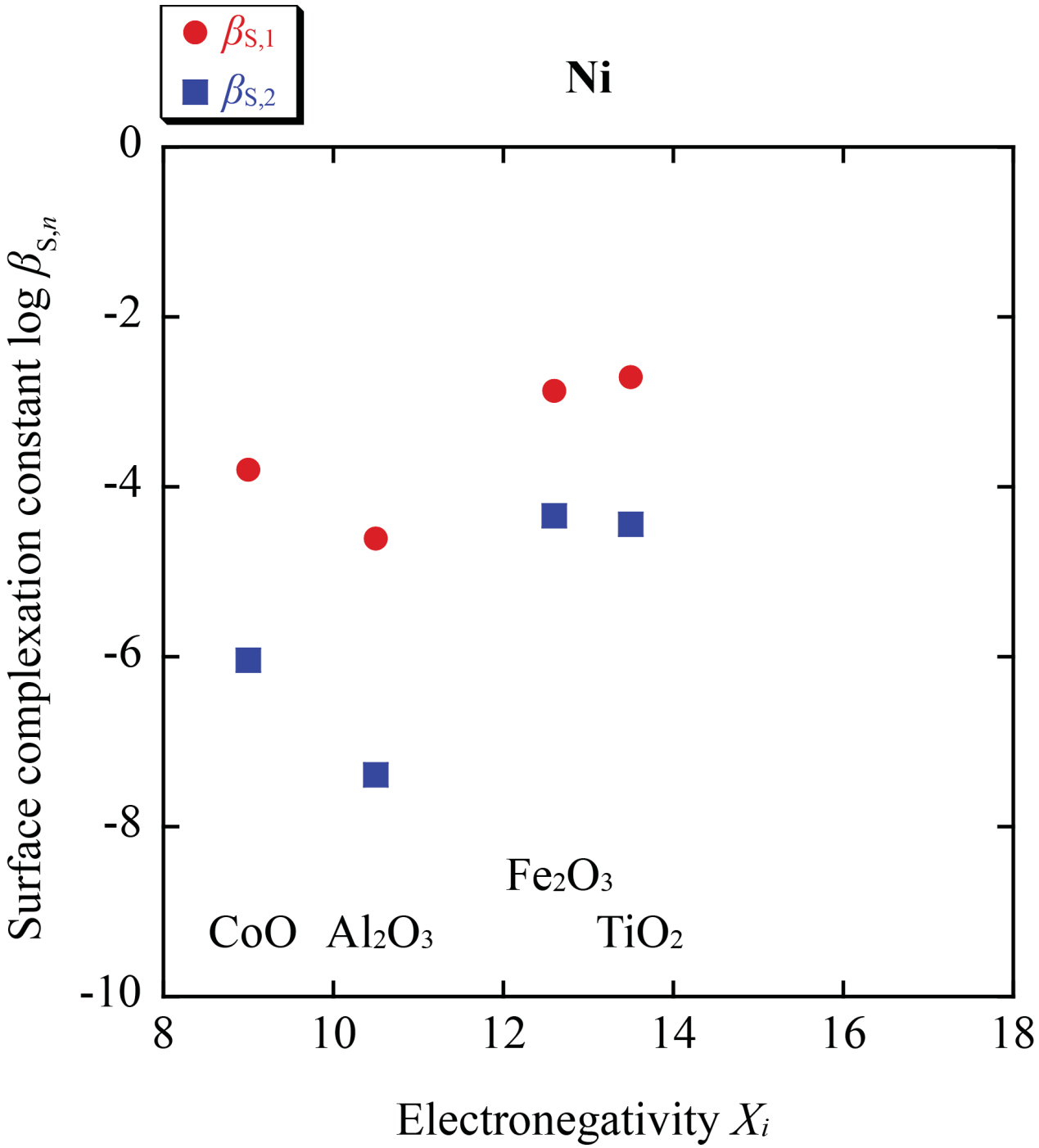

Fig. 24. Plots of surface complexation constants for the distribution of Ni(II) on metal oxide nanoparticles in water as a function of X_i for metal oxide nanoparticles according to Eq. (22).

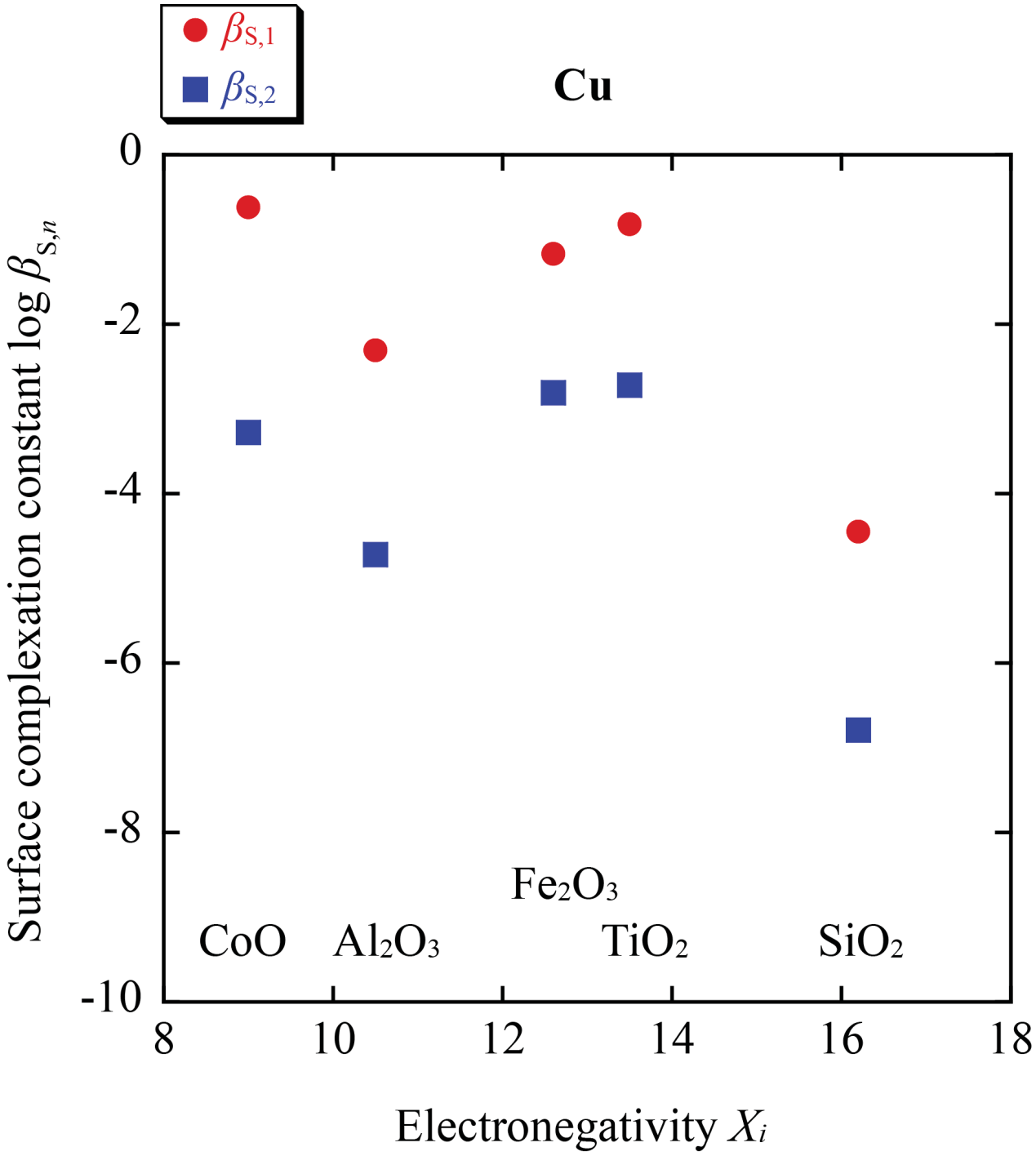

Fig. 25. Plots of surface complexation constants for the distribution of Cu(II) on metal oxide nanoparticles in water as a function of X_i for metal oxide nanoparticles according to Eq. (22).

the $\beta_{S,n}$ values of Be(II) decrease with an increase of X_i, indicating that the contribution of the coordination of >S-O$^-$ to Be^{2+} exceeds that of the deprotonation of >S-OH. This may reflect the relatively strong interaction between the small Be^{2+} ion and >S-O$^-$. The appearance of the maximum in the complexation constant at X_i = 13 (Fe_2O_3) is a result of the competition of the two different processes (Eqs. (20) and (21)). In the case of Ni(II) and Cu(II), except CoO, the similar correlation between X_i and the complexation constants is observed as shown in Figs. 24, and 25.

The complexation constants of CoO with Ni(II) and Cu(II) are greater than those expected from the above tendency. This shows the specific stability of the complexes of Ni(II) and Cu(II) on the CoO surface. When the difference of the effective ionic radii of the metal-oxide metal atom and the metal ion bound to the metal oxide is small, the structural distortion of the complex becomes small and the complex should be stabilized. The ionic radii of the metal-oxide metal atom and the metal ion and the difference of these ionic radii are summarized in Table 6.[42] Herein, the coordination number of the metal-oxide metal atom is regarded as 6 for Al(III), Ti(IV), Fe(III), and Co(II); 4 for Si(IV) and Cu(II), considering the crystal structures.[43] The coordination number of the metal ion bound to the metal oxide is 4 for Be(II); 6 for Ni(II); 4 and 6 for Cu(II). As shown in Table 6, the difference in the ionic radii between Co(II) and Ni(II) is very small and that between Co(II) and Cu(II) (coordination number 6) is also very small. Therefore, the oxide nanoparticle is favorable to the complexation with the metal ion which has an ionic radius close to that of the metal-oxide metal atom.

Here, the following discussion focuses on SiO_2 nanoparticle. As mentioned above, in the higher X_i region, the $\beta_{S,n}$ values decrease with an increase of X_i. In Figs. 23 and 25, the extent of the decrease the $\beta_{S,n}$ values is smaller for Be(II) than for Cu(II). This result can be explained by considering the difference of the ionic radii. The ionic radius of Si(IV) is similar to that of Be(II). Thus, the complexation constants of SiO_2 with Be(II) are greater than those expected from the above tendency. Therefore, the extent of the decrease the $\beta_{S,n}$ values is smaller for Be(II) than for Cu(II).

Table 6. Differences of the effective ionic radii of the metal-oxide metal atom and the metal ion bound to the metal oxide*

	Difference of ionic radii (Å) Metal ion bound to metal oxide			
Metal oxide	Be(II)	Ni(II)	Cu(II) (CN:4)	Cu(II) (CN:6)
Al_2O_3	0.265	0.155	0.035	0.195
SiO_2	0.010	0.430	0.310	0.470
TiO_2	0.335	0.085	0.035	0.125
Fe_2O_3	0.375	0.045	0.075	0.085
CoO	0.475	0.055	0.175	0.015
CuO	0.300	0.120	0	0.160

Effective ionic radii used for the calculations (ref. 42): Be(II) 0.27 Å for coordination number (CN) 4 ; Al(III) 0.535 Å for CN 6 ; Si(IV) 0.26 Å for CN 4 ; Ti(IV) 0.605 Å for CN 6 ; Fe(III) 0.645 Å for CN 6 ; Co(II) 0.745 Å for CN 6 ; Ni(II) 0.69 Å for CN 6 ; Cu(II) 0.57 Å for CN 4 ; Cu(II) 0.73 Å for CN 6.

4. Conclusions

The purpose of this study is to clarify the partition behavior of metal ions to metal oxide nanoparticles dispersed in water. The partition behavior was quantitatively evaluated and explained on the basis of the complexation model between metal ion and surface hydroxyl sites of the oxides. The metal ions used were Be(II), Ni(II), and Cu(II). The nanoparticles used were Al_2O_3, SiO_2, TiO_2, Fe_2O_3, CoO, and CuO.

The distribution ratio of the metal ions to the nanoparticles was evaluated. For all the oxide nanoparticles, the *D* values vary with the nanoparticles and increase with increasing pH. In addition, the zeta potentials and particle size distributions of the nanoparticles dispersed in water were measured. The order of these values are not consistent with that of the *D* value of the metal ions with the metal oxide nanoparticles. It appears that these values of the oxide nanoparticles are not dominant factors determining their reactivity for the metal ions.

From these results, the partition of the metal ion to the metal oxides was evaluated based on the surface complexation model, in which the surface hydroxyl sites on the oxides deprotonate and form complexes with the metal ion in water. By analyzing the pH dependence of the distribution ratio, the surface complexation constants $\beta_{S,n}$ (n represents the number of the surface $-O^-$ groups bound to one metal ion) were determined. In general, one metal ion reacts with one or two hydroxyl sites on the oxide surface.

The differences of the complexation constants depending on the type of CuO nanoparticles were discussed. The $\beta_{S,2}$ values are similar for all four kinds of CuO nanoparticles. On the other hand, the $\beta_{S,3}$ values vary with the kind of CuO nanoparticles. The dependence of the complexation constant on the kind of CuO nanoparticles can not be clearly explained at the present stage.

The differences of the complexation constants among the metal ions were discussed. Except for CoO, the $\beta_{S,n}$ value increases with an increase of the hydrolysis constants for the metal ions. This result supports that the surface hydroxyl sites are concerned with the complexation of the metal ions on the oxide nanoparticles.

The differences of the complexation constants among the oxide nanoparticles were discussed. The complexation constants were found to vary with the electronegativity X_i of the metal (or Si) composing the oxide. The fact that the complexation constants show maximum values for Fe_2O_3 can be explained based on the opposite effects of the charge density of the oxygen atom on the deprotonation of the surface hydroxyl sites and on the binding of the negatively charged deprotonated site to the metal ion.

In addition, the oxide nanoparticles are favorable to the complexation with the metal ion which has an ionic radius close to that of the metal-oxide metal atom. The structural distortion of the complex becomes small and the complex should be stabilized. This tendency is shown by the fact that the complexation constants of Ni(II) and Cu(II) with CoO and that of Be(II) with SiO_2 are greater than those expected from the above tendency.

As can be seen from Eq. (15), the distribution ratio of the metal ions between the nanoparticle phase and the aqueous solution phase depends not only on the surface complexation constants but also on the surface hydroxyl concentration (amount of -OH sites per unit mass of the particles). For example, the higher distribution ratio of Be(II) for CoO than for CuO–CIK is explained in terms of the higher surface hydroxyl concentration of CoO. Nanoparticles of the oxides, which have extremely large specific surface area-to-weight ratios, exhibit high adsorption ability for metal ions because of their high surface hydroxyl concentration. And the distribution ratio can be estimated using the complexation constants and the surface hydroxyl concentration.

It can be concluded that the electronegativity (X_i) of the lattice metal ions of oxide is the dominant factor determining the partition behavior of metal ions to metal oxide nanoparticles. The next step would be to clarify a second dominant factor. These findings would not only clarify the behavior of radionuclides in cooling water but also apply to the scavengers of metal ions.

5. References

1) R. P. Feynman, *Engineering and Science*, **1960**, *23*, 5, 22−36.
2) M. Fernández-García, A. Martínez-Arias, J. C. Hanson, J. A. Rodríguez, *Chem. Rev.*, **2004**, *104*, 4063−4104.
3) M. A. Carpenter, S. Mathur, A. Kolmakov, "*Metal Oxide Nanomaterials for Chemical Sensors*", Springer, **2012**.
4) A. Heller, *Acc. Chem. Res.*, **1995**, *28*, 503−508.
5) A. L. Linsebigler, G. Q. Lu, J. T. Yates, *Chem. Rev.*, **1995**, *95*, 735−758.
6) P. Poizot, S. Laruelle, S. Grugeon, L. Dupont, J.-M. Tarascon, *Nature*, **2000**, *407*, 496−499.
7) M. Kole, T. K. Dey, *Exp. Therm. Fluid Sci.*, **2010**, *34*, 6, 677−683.
8) M. Mahmoudi, S. Sant, B. Wang, S. Laurent, T. Sen, *Adv. Drug Delivery Rev.*, **2011**, *63*, 24−46.
9) L. Momtazia, S. Bagherifama, G. Singhb, A. Hofgaardc, M. Hakkarainend, W. R. Glommf, N. Roosc, G. M. Mælandsmoe, G. Griffithsc, B. Nyström a, *J. Colloid Interface Sci.*, **2014**, *433*, 76−85.
10) C. Burda, X. Chen, R. Narayanan, M. A. El-Sayed, *Chem. Rev.*, **2005**, *105*, 1025−1102.
11) A. Zabet-Khosousi, A.-A. Dhirani, *Chem. Rev.*, **2008**, *108*, 4072−4124.
12) M. Hua, S. Zhang, B. Pan, W. Zhang, L. Lv, Q. Zhang, *J. Hazard. Mater.*, **2012**, *211−212*, 317−331.
13) C.-Y. Cao, J. Qu, W.-S. Yan, J.-F. Zhu, Z.-Y. Wu, W.-G. Song, *Langmuir*, **2012**, 28, 4573−4579.
14) G. E. Brown Jr., G. A. Parks, *Int. Geol. Rev.*, **2001**, *43*, 963−1073.
15) W. Stumm, J. C. Westall, R. Parsons, J. A. Marinsky, P. W. Shindler, H. Motschi, G. H. Bolt, W. H. Van Riemsdijk, W. Schneider, B. Schwyn, G. Furrer, A. T. Stone, J. J. Morgan, A. E. Blum, A. C. Lasaga, J. Schott, J.-C. Petit, L. Sigg, J. Buffle, R. S. Altmann, C. R. O'Melia, F. M. M. Morel, P. M. Gschwend, R. G. Zepp, N. L. Wolfe, M. Whitfield, D. R. Turner, W. S. Fyfe, "*Aquatic Surface Chemistry-Chemical Processes at the Particle-Water Interface*",

Wiley-Interscience, New York, **1987**.

16) J. A. Davis, D. B. Kent, *Reviews in Mineralogy and Geochemistry*, **1990**, *23*, 177−260.

17) D. A. Sverjensky, *Geochimica et Cosmochimica Acta*, **2006**, *70*, 2427−2453.

18) R. Rahnemaie, T. Hiemstra, W. H. van Riemsdijk, *J. Colloid Interface Sci*., **2006**, *297*, 379−388.

19) L. Balistrieri, P. G. Brewer, J.W. Murray, *Deep-Sea Res*., **1981**, *28A*, 101−121.

20) S. Itoh, T. Miura, M. Furusaka, S. Yasui, Y. Ogawa, Y. Kiyanagi, S. Sasaki, K. Iijima, in Proceedings of the 14th Meeting of the International Collaboration on Advanced Neutron Sources (ICANS-XIV), **1998**, Utica, Illinois, USA, 823.

21) H. Matsumura, N. Kinoshita, A. Toyoda, K. Masumoto, K. Bessho, M. Hagiwara, Y. Yamanoi, *Nucl*. *Technol*., **2009**, *168*, 979.

22) K. Bessho, H. Matsumura, N. Kinoshita, K. Masumoto, H. Monjushiro, M. Taira, M. Sato, M. Sawabe, A. Komiya, Y. Oki, S. Shimada, S. Katsuta, in Proceedings of the 11th Workshop on Environmental Radioactivity (KEK Proceedings 2010-8), **2010**, Tsukuba, Ibaraki, Japan, 19 (in Japanese).

23) K. Bessho, H. Matsumura, M. Hagiwara, K. Takahashi, A. Takahashi, H. Iwase, K. Masumoto, H. Monjushiro, Y. Oyama, T. Sekiguchi, Y. Yamada, in Proceedings of the 11th Meeting of the Task-Force on Shielding Aspects of Accelerators, Targets, and Irradiation Facilities (SATIF-11), **2013**, Tsukuba, Ibaraki, Japan, 61.

24) H. Matsumura, S. Sekimoto, H. Yashima, A. Toyoda, Y. Kasugai, N. Matsuda, K. Oishi, K. Bessho, Y. Sakamoto, H. Nakashima, D. Boehnlein, G. Lauten, A. Leveling, N. Mokhov, K. Vaziri, *Prog*. *Nucl*. *Sci*. *Technol*., **2014**, *4*, 372.

25) K. Bessho, Y. Oki, N. Akimune, H. Matsumura, K. Masumoto, S. Sekimoto, N. Osada, N. Kinoshita, H. Monjushiro, S. Shibata, *J. Radioanal*. *Nucl*. *Chem*., in press.

26) K. Bessho, H. Matsumura, A. Takahashi, K. Masumoto, *J. Radioanal*. *Nucl*. *Chem*., in press.

27) Compact Tabletop Centrifuge Model 2010 specifications (KUBOTA Corporation), (http://www.centrifuge.jp/products/discontinued-model-2010/)

28) Micro Refrigerated Centrifuge Model 3700 specifications (KUBOTA

Corporation),
(http://www.centrifuge.jp/products/model-3700/)

29) R. W. Baker, "*Membrane Technology and Applications*, *2nd ed*.", John Wiley & Sons, West Sussex, **2004**.

30) SZ-100 nano Partica specifications (HORIBA, Ltd.),
(http://www.horiba.com/scientific/products/particle-characterization/particle-size-analysis/details/sz-100-7245/)

31) K. Tanabe, "*Solid Acids and Bases Their Catalytic properties*", Academic Press Inc., New York, **1971**.

32) G. Schwarzenbach, H. Wenger, *Helv*. *Chim*. *Acta*, **1969**, *52*, 644−665.

33) E. Chinea, S. Dominguez, A. Mederos, F. Brito, A. Sanchez, A. Ienco, A. Vacca, *Main Group Metal Chem*., **1997**, *20*, 11−17.

34) Yu. F. Orlov, E. I. Belkina, *Russ*. *J*. *Inorg*. *Chem*., **2011**, *56*, 6, 975−980.

35) D. T. Richens, "*The Chemistry of Aqua Ions: Synthesis, Structure and Reactivity: A Tour Through the Periodic Table of the Elements*", Wiley, **1997**.

36) H. Tamura, K. Mita, A. Tanaka, and M. Ito, *J. Colloid Interface Sci*., **2001**, *243*, 202−207.

37) K. Tanaka, A. Ozaki, *J. Catal*., **1967**, *8*, 1−7.

38) L. Pauling, "*The Nature of the Chemical Bond*" 3rd ed., Cornell Univ. Press, New York, **1960**.

39) K. Tanaka, A. Ozaki, *Bull*. *Chem*. *Soc*. *Jpn*., **1968**, *41*, 2812−2813.

40) B. Imelik, C. Naccache, G. Coudurier, Y. B. Taarit, J. C. Vedrine, "*Catalysis by Acids and Bases*", Elsevier, Amsterdam, London, New York, **1985**.

41) H. Tamura, N. Katayama, R. Furuichi, *J. Colloid Interface Sci*., **1997**, *195*, 192−202.

42) R. D. Shannon, *Acta Cryst*., **1976**, *A32*, 751−767.

43) K. Tanabe, T. Seiyama, K. Hueki, "*Metal Oxides and Complex Oxides The Correlation with Their Preparation, Properties, Structure, Catalysis, and Inorganic Material.*", Kodansha Scientific, Japan, **1978** (in Japanese).

6. Acknowledgement

I would like to express my deepest appreciation and gratitude to my supervisor, Associate professor Shoichi Katsuta whose enormous help and face-to-face discussion are invaluable during the course of my study. In addition, I extend my appreciation to all members of the Katsuta Lab. for their considerable assistance and support.

The suggestions of Professor Hirofumi Kanoh for his practical advice, Professor Hideo Togo for his valuable comment, Professor Fumio Sakane for his sincere encouragement, Associate professor Yoshihiro Kudo for his insightful comment, and Associate professor Chiya Numako for her considerable encouragement are very helpful in clarifying the thesis.

I would like to show my greatest appreciation and gratitude to Associate professor Kotaro Bessho at High-Energy Accelerator Research Organization (KEK) whose considerable encouragement and constructive advice are invaluable during the course of my study.

The suggestion of Professor Hideaki Monjushiro at KEK for incisive comment and sincere encouragement is very helpful. In addition, I extend my appreciation to all members of the Radiation Science Center, KEK for their continuous assistance and support.

I would like to express my heartfelt gratitude to Mr. Taichi Koyanagi of CIK NanoTek Corporation. The TEM photographs of NanoTek® (Fig. 1) are quoted by kind permission of CIK NanoTek Corporation.

Without their persistent help, this thesis would not have been materialized.

Finally, I express all my respects and deep appreciation to all my family and friends.